

**POLYSULFONE/CARBIDE DERIVED CARBON MIXED
MATRIX MEMBRANE FOR SEPARATION OF CO₂ FROM
NATURAL GAS**

BY

MUSA OLAJIDE NAJIMU

A Thesis Presented to the
DEANSHIP OF GRADUATE STUDIES

KING FAHD UNIVERSITY OF PETROLEUM & MINERALS

DHAHRAN, SAUDI ARABIA

1963 ١٣٨٣

In Partial Fulfillment of the
Requirements for the Degree of

MASTER OF SCIENCE

In

CHEMICAL ENGINEERING

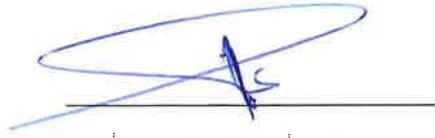
JUNE 2017

KING FAHD UNIVERSITY OF PETROLEUM & MINERALS

DHAHRAN- 31261, SAUDI ARABIA

DEANSHIP OF GRADUATE STUDIES

This thesis, written by **NAJIMU MUSA OLAJIDE** under the direction of his thesis advisor and approved by his thesis committee, has been presented and accepted by the Dean of Graduate Studies, in partial fulfillment of the requirements for the degree of **MASTER OF SCIENCE IN CHEMICAL ENGINEERING**



Dr. **Isam Al-Jundi**
(Advisor)



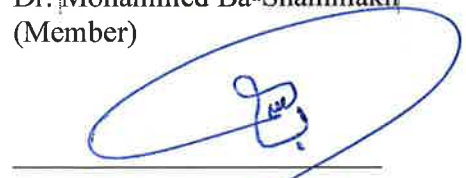
Dr. **Mohammed Ba-Shammakh**
Department Chairman



Dr. **Mohammed Ba-Shammakh**
(Member)



Dr. **Salam A. Zummo**
Dean of Graduate Studies



Dr. **Basim Abussaud**
(Member)

16/07/2017

Date



© Najimu Musa Olajide

2017

[To my parents for their sacrifice |

ACKNOWLEDGMENTS

All praises and gratitude be to Allah for the gift of life, without which there wouldn't be any me to embark on this work. May the peace and blessings of Allah be upon His prophet Mohammad.

I would like to acknowledge all the support and guidance of my advisor, Dr Isam Al-Jundi. His patience and immense contributions in form of great ideas and problem solving are highly appreciated. I equally thank my committee members, Dr Basim Abussaud and Dr Mohammed Ba-Shammakh for their time and great assistance in improving the quality of my work. Also appreciated is the technical support of Mr Syed Amanullah of chemical engineering department and support on characterizations by Mr Mohammed Abdelaziz Elgzoly of chemical engineering department.

On my appreciation list are all my professors at KFUPM, the rigorous training while taking courses is highly appreciated. To my colleagues such as KAZEEM Taye Saheed and others, I am grateful for their support, inspirations and help throughout my stay in KFUPM.

I would never miss to acknowledge my parents whose sacrifice, patience, love and prayers are what give me the opportunity to move on in life; all of these are highly acknowledged. My wife, Karimot Yinusa and my son, Abdullah Musa patiently stood by me while completing this work, their patience and encouragements are as well highly appreciated.

To KFUPM, I say thank you for the admission opportunities. And to the Kingdom of Saudi Arabia, I say thank you for the scholarship opportunities. |

TABLE OF CONTENTS

ACKNOWLEDGMENTS	V
TABLE OF CONTENTS.....	VI
LIST OF TABLES	IX
LIST OF FIGURES	X
LIST OF ABBREVIATIONS.....	XII
ABSTRACT.....	XIII
ملخص الرسالة	XV
CHAPTER 1 INTRODUCTION.....	1
1.1 Saudi Arabia Natural Gas Overview.....	3
1.2 Natural Gas Pretreatment	6
1.3 The need for removal of CO ₂	8
1.4 CO ₂ removal technologies and processes.....	8
1.4.1 Absorption.....	8
1.4.2 Adsorption.....	9
1.4.3 Cryogenics.....	9
1.4.4 Membrane Gas separation.....	9
1.5 Advantages of membrane system	11
1.6 Performance requirements for membrane materials.....	12
1.7 Mixed matrix membrane	12
1.8 Carbide derived carbon (CDC)	13

1.9	Research objectives.....	17
CHAPTER 2 LITERATURE REVIEW.....		19
2.1	Introduction to gas membranes.....	19
2.2	Gas membrane formation.....	21
2.2.1	Wet phase inversion	21
2.2.2	Dry phase inversion.....	21
2.2.3	Dry/wet Phase inversion.....	22
2.3	Fundamentals of Gas separation membranes	23
2.4	Commercial membrane and membrane processes.....	24
2.5	Mixed matrix membrane for CO ₂ separation	25
CHAPTER 3 METHODOLOGY.....		36
3.1	Materials.....	36
3.2	Membrane Preparation	36
3.2.1	Loading Range	39
3.3	Characterization of membrane samples.....	41
3.3.1	Scanning Electron Microscopy	41
3.3.2	X-ray diffraction	41
3.3.3	Fourier Transform Infrared Spectroscopy (FTIR)	42
3.3.4	Thermogravimetric analysis (TGA).....	45
3.4	Gas Permeation.....	45
3.4.1	Temperature range	47
3.4.2	Pressure range.....	48
CHAPTER 4 RESULTS AND DISCUSSIONS		49
4.1	Characterizations	49

4.1.1	Scanning Electron Microscopy	49
4.1.2	X-ray diffraction	53
4.1.3	Fourier Transform Infrared Spectroscopy (FTIR) results.....	55
4.1.4	Thermogravimetric analysis TGA	64
4.2	Gas permeation.....	67
4.2.1	Effect of polymer concentration.....	67
4.2.2	Effect of loading	69
4.2.3	Effect of temperature	72
4.2.4	Effect of pressure	74
CHAPTER 5 CONCLUSIONS AND RECOMMENDATIONS.....		76
5.1	Conclusions	76
5.2	Recommendations.....	77
REFERENCES		78
VITAE.....		90

LIST OF TABLES

Table 1: Typical composition of natural gas[3]	4
Table 2: U.S. National Pipeline Grid’s Natural Gas Composition Specifications for Delivery	7
Table 3: Intrinsic permeation properties of polysulfone [32]	17
Table 4: Review summary	34
Table 5: Compositions of casting solutions	38
Table 6: Filler loading in mixed matrix membrane	39
Table 7: Aliphatic hydrocarbons characteristic infrared bands	43
Table 8: Aromatic compounds characteristic infrared bands	44
Table 9: Peak Identification of CDC FTIR.....	59
Table 10: Major Peaks of PSF FTIR spectra	62
Table 11: TGA data for CDC and membrane samples	66

LIST OF FIGURES

Figure 1: Middle East end-use sector natural gas consumption, 2012-40	2
Figure 2: World proven natural gas reserves	3
Figure 3: Pretreatment of natural gas	7
Figure 4: Solution diffusion mechanism of dense membrane.	10
Figure 5: Structures of gas separation membranes (a) integrally skinned asymmetric; (b) multicomponent ('cauked'); (c) single layer thin-film composite; (d) multilayer thin-film composite; (e) asymmetric composite.	20
Figure 6: Schematic representation of phase inversion techniques - (a) dry phase inversion (b) wet phase inversion (c) dry/wet phase inversion	23
Figure 7: schematic diagram of permeation equipment.....	46
Figure 8: Phase diagram of CO ₂	47
Figure 9: Surface SEM images of membrane samples at magnification of 20,000 – (a) Pure PSF membrane, (b) 0.1 wt% PSF/CDC membrane, (c) 0.5 wt% PSF/CDC membrane, (d) 1.0 wt% PSF/CDC membrane and (b) 2.0 wt% PSF/CDC membrane	51
Figure 10: Cross section SEM images of membrane samples at magnification of 10,000– (a) Pure PSF membrane, (b) 0.1 wt% PSF/CDC membrane (c) 0.5 wt% PSF/CDC membrane, (d) 1.0 wt% PSF/CDC membrane and (b) 2.0 wt% PSF/CDC membrane	52
Figure 11: XRD pattern of CDC.....	54
Figure 12: XRD patterns for pure membrane and mixed matrix membranes.....	55
Figure 13: FTIR Spectra of CDC.....	57

Figure 14: (a)Schematic illustration of the selective chlorination of a metal carbide lattice with a fcc structure [67], (b) CDC model showing surface chemistry, (c) chemical structure of PSF.	60
Figure 15: FTIR spectra of pure membrane and MMM	61
Figure 16: TGA curves of pure and mixed matrix membrane.....	65
Figure 17: Effect of PSF concentration on gas permeance and selectivity.....	69
Figure 18: Effect of CDC loading on permeance and selectivity	71
Figure 19: Effect of temperature on gas permeance and selectivity of 1 wt% MMM.....	73
Figure 20: Effect of feed pressure on performance of 1 wt% mixed matrix membrane.....	75

LIST OF ABBREVIATIONS

MMM	:	Mixed matrix membrane
PSF	:	Polysulfone
CDC	:	Carbide derived carbon
NMP	:	1-Methyl-2-pyrrolidinone
THF	:	Tetrahydrofuran
SEM	:	Scanning Electron Microscopy
XRD	:	X-ray Diffraction
FTIR	:	Fourier Transform Infrared Spectroscopy
TGA	:	Thermogravimetric Analysis

ABSTRACT

Full Name : [Musa Olajide Najimu]
Thesis Title : [Polysulfone/carbide derived carbon mixed matrix membrane for separation of CO₂ from natural gas]
Major Field : [Chemical Engineering]
Date of Degree : [May, 2017]

For the purpose of continued competition of membrane technology with other processes and consequently in the search for high performance gas membrane, mixed matrix membranes are being considered in replacement of polymeric membranes. In this study, we have investigated the development of mixed matrix membrane comprising PSF and carbide derived carbon (CDC) nanoparticles for the separation of CO₂ from natural gas. Firstly, the formulation of the pure PSF membrane was optimized using the dry/wet phase inversion membrane preparation technique; this resulted in the critical concentration of 30 wt% PSF in the mixture of solvents (NMP/THF) and non-solvent (ethanol). Consequently, mixed matrix membranes were prepared by dispersing CDC nanoparticles at different concentrations in the optimized pure PSF membrane formulation. XRD, TGA, SEM and FTIR characterizations respectively confirmed the unchanged amorphous nature of the membrane, reinforced thermal stability, uniform dispersion up to 0.5 wt% loading and imparted polarity due to the favourable surface chemistry of CDC. Membrane performance evaluation by gas permeation tests revealed the enhancement in CO₂ permeance by 120% achieved from the 0.5 wt% mixed matrix membrane as a result of the simultaneous enhanced solubility due to polarity and enhanced diffusivity due to creation of diffusivity channels by the nanoporous CDC.

However, the best CO₂/CH₄ selectivity of 27 was obtained from the 1 wt% mixed matrix membrane; this may be attributed to the formation of optimum CDC cluster size which favored both solubility selectivity and diffusivity selectivity. Furthermore, operating temperature effect studies showed that the laboratory temperature (20 °C) was the best operating temperature of the 1 wt% mixed matrix membrane while the low pressure effect studies predicted better performance for the 1 wt% mixed matrix membrane at higher feed pressures. |

ملخص الرسالة

الاسم الكامل: موسى أولاجيدي ناجيمو

عنوان الرسالة: إستخدام خليط أغشية بوليسولفون/الكربيد المشتق من الكربون لفصل غاز ثاني أكسيد الكربون من الغاز الطبيعي

التخصص: الهندسة الكيميائية

تاريخ الدرجة العلمية: مايو 2017

نسبة للمنافسة المستمرة بين مجالات تقنيات الأغشية والعمليات الأخرى وكنتيجة للبحث عن أغشية غازية عالية الأداء، أعتبرت حشوات الأغشية المخلوطة كبديل لأغشية البوليمرات. في هذه الدراسة، لقد قمنا بتطوير خليط أغشية هي عبارة عن خليط من PSF وجزئيات الكربيد متناهية الصغر المستمدة من الكربون (CDC) لأغراض فصل غاز ثاني أكسيد الكربون (CO_2) من خليط الغازات الطبيعية. أولاً، تم تحسين صيغة أغشية PSF النقية بإستخدام عمليات تحضير أغشية الطور الجاف/الرطب العكسية؛ من هذه الدراسة تم الوصول الى التركيز الحرج لـ PSF وهو 30% تركيز وزني في خليط المذيبات (NMP/THF) و اللامذيبات (ethanol). كنتيجة لذلك تم تجهيز خط الأغشية بإضافة جزئيات CDC متناهية الصغر بتركيز مختلفة الى التركيز المثالي لـ PSF. تقنيات XRD، TGA، SEM، و FTIR اثبتت أنه لا يوجد تغير في الطبيعة الغير متبلرة للغشاء المطور، كما أكدت الثبات الحراري للغشاء، وأن التشتت الموحدة يصل إلى 0.5% بالوزن بسبب الكيمياء السطحية الملائمة لـ CDC. تقييم أداء الأغشية عن طريق إختبارات تغلغل الغاز أظهرت تحسن كبير في تغلغل غاز ثاني أكسيد الكربون وصل

لـ 120% عند إستخدام خليط الأغشية ذو التركيز 0.5% تركيز وزني كنتيجة لتحسين الذوبانية نتيجة للاستقطاب وتعزيز الانتشارية بسبب إنشاء قنوات الانتشارية من قبل جزئيات CDC متناهية الصغر. ومع ذلك، تم الحصول على أفضل انتقائية CO_2/CH_4 من 27 عند إستخدام خليط أغشية ذات تركيز 1% بالوزن؛ ويمكن أن يعزى ذلك إلى تشكيل الحجم الأمثل لكتلة الـ CDC التي حققت كلا من الذوبان والانتقائية الأمثل. وعلاوة على ذلك، أظهرت دراسات تأثير درجة حرارة التشغيل أن درجة حرارة المختبر (20 درجة مئوية) هي أفضل درجة حرارة تشغيل عند

إستخدام تركيز 1% بالوزن في حين أن دراسات تأثير الضغط المنخفض توقع أداء أفضل لتركيز 1% بالوزن عند إستخدام ضغوط تغذية عالية.

CHAPTER 1

INTRODUCTION

The world uses about 100 trillion standard cubic feet of natural gas every year [1]. It is an important commodity that is used as either fuel or chemical feed stock in sectors such as residential, commercial, electric generation, industrial and transportation. Figure 1 shows that Industrial use and electric power generation are the areas for which natural gas is widely used in the Middle East. Natural gas is found all around the world, with the largest reserves in the former soviet union and the Middle East [2] as shown in Figure 2, but Saudi Arabia with proven natural gas reserves of over 250 trillion cubic feet (7 trillion cubic metres) is known to have one of the largest reserves in the gulf [1].

Natural gas typically consists of mainly methane and also some amount of ethane, propane and butane. It also contains undesirable components such as water, carbon dioxide, nitrogen, and hydrogen sulfide [1]. Trace quantities of hydrogen, argon and helium may also be present, together with some aromatics such as xylene, toluene and benzene which are toxic. Certain contaminants such as carbon disulfide (CS_2), carbonyl sulfide (COS) and mercaptans—R-SH may be present in small quantities [2]. Mercury can also exist in natural gas either as an organometallic compound in liquid fractions or as a metal in vapor phase. A typical composition of natural gas shown in Table 1 reveals the composition range of constituents of natural gas and it shows that for instance, the composition of CO_2 in natural gas ranges from 0 to 42.66 [3].

Based on careful forecast, natural gas consumption will have the highest rate of growth among other types of fossil fuels. Its demand is based on key growth factors which include its lower emissions of CO₂, its safer and more reliable generation of power than nuclear, increase in residential and industrial use as a result of population growth and low cost [3].

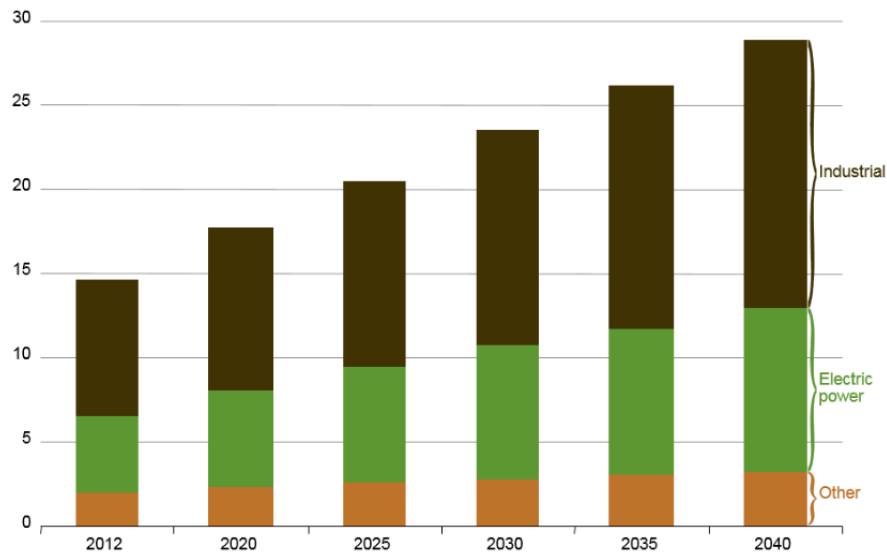


Figure 1: Middle East end-use sector natural gas consumption, 2012-40

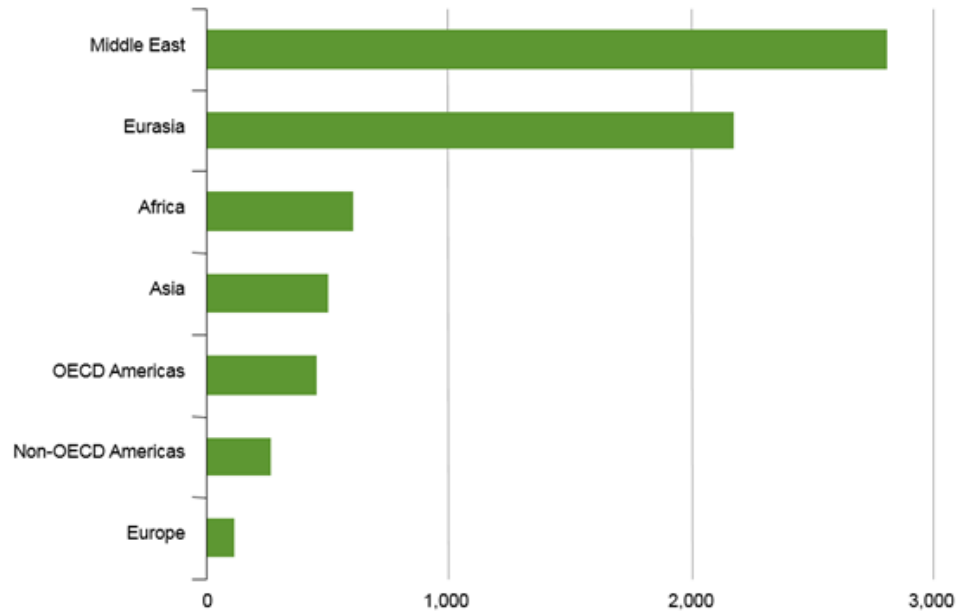


Figure 2: World proven natural gas reserves

1.1 Saudi Arabia Natural Gas Overview

Since the discovery of natural gas in Saudi Arabia, there has been a rapid increase in gas production. All exploration, drilling and production activities in the Kingdom are done by Saudi Aramco. Through joint ventures with Saudi Aramco, international oil companies also operate in Saudi oil fields and refineries [4].

Saudi Arabia is known to have the fifth largest reserves of natural gas in the world with production ratio of 81 years [5]. In 2015, about 11.6 billion scfd of raw gas processing was recorded by Saudi Aramco[6]. The surge in production was as a result of development and exploration of increasing number of discovered oil and gas fields. As at 2015, Saudi Arabia Kingdom Master Gas system has a throughput of 9.3 billion scfd of sales gas. The Master Gas System was constructed in 1975 for the utilization of the

natural gas for economic advantage. Being a gas distribution network, it delivers natural gas as a feedstock to petrochemical plants spread across the industrial cities of Yanbu on the Red Sea and Jubail [7]. Prior to the advent of the Master Gas System, all of Saudi Arabia's natural gas output was previously flared [5].

Table 1: Typical composition of natural gas[3]

Typical Gas Compositions

	Canada (Alberta)	Western Colorado	Southwest Kansas	Bach Ho Field ^a Vietnam	Miskar Field Tunisia	Rio Arriba County, New Mexico	Cliffside Field, Amarillo, Texas
Helium	0.0	0.0	0.45	0.00	0.00	0.0	1.8
Nitrogen	3.2	26.10	14.65	0.21	16.903	0.68	25.6
Carbon dioxide	1.7	42.66	0.0	0.06	13.588	0.82	0.0
Hydrogen sulfide	3.3	0.0	0.0	0.00	0.092	0.0	0.0
Methane	77.1	29.98	72.89	70.85	63.901	96.91	65.8
Ethane	6.6	0.55	6.27	13.41	3.349	1.33	3.8
Propane	3.1	0.28	3.74	7.5	0.960	0.19	1.7
Butanes	2.0	0.21	1.38	4.02	0.544	0.05	0.8
Pentanes and heavier	3.0	0.25	0.62	2.64	0.630	0.02	0.5

^a Tabular mol% data is on a wet basis (1.3 mol% water)

Based on Saudi Aramco forecasts, it is expected that natural gas demand in the Kingdom will almost double by 2030 from 2011 levels of 3.5 trillion cubic feet (Tcf) per year [5]. Apart from supply as feedstock to petrochemical companies, increase in demand of gas arises from aim to reduce the Kingdom's reliance on liquid fuel for electricity generation and to power seawater desalination plants [6]. As a result of this, part of Saudi Arabia's commitments is to double its natural gas production by 2030 in order to meet the rising

domestic demand [7]. Over 45% of the domestic energy demand comes from natural gas. In order to achieve the vision 2030 target, Saudi Aramco is expanding its collaborations with more private companies through joint ventures to ensure discoveries and development of additional gas fields. Because majority of the gas is associated with petroleum deposit [5], expansion is also extending to non-associated gas fields to avoid gas production being tied to production of oil and to further boost gas production. For instance, five gas fields (Abu Ali, Faras, Amjad, Badi, and Faris) and one oil and gas field (Qadqad) and two oil fields (Sadawi and Naqa) were discovered by Aramco in 2014, making the highest number of discoveries in the company's history and bringing the total number of discovered fields to 129 [8, 9]. During 2015, five new oil and gas fields were discovered, raising the total number of discovered oil and gas fields in the Kingdom to 134 [6]. Also recently, the national company began gas production at the offshore Hasbah field [10]. In addition to discovery and development of gas fields, more gas plants are being constructed in order to accommodate processing of gas from the newly discovered fields and to serve specific purpose. Saudi Aramco's latest gas plant, Wasit, is designed to process 2.5 billion scfd of nonassociated gas and supply 1.7 billion scfd of sales gas to the Master Gas System and it is expected to generate 798 megawatts of power by cogeneration. Midyan gas plant is anticipated to come onstream by the end of 2016 when it will deliver sales gas and condensate to power the Saudi Electricity Company's new Duba Power Plant while Fadhili gas plant with the cogeneration capacity to produce roughly 1.3 gigawatts of power and 3.2 million pounds per hour of steam will be onstream by 2019 [6].

Saudi Arabia does not import or export natural gas, the entire gas production in the country is domestically consumed. The gas is being used for desalination, re-injection, power generation as well as feedstock to petrochemical plants [7].

1.2 Natural Gas Pretreatment

Raw natural gas stream has to be treated to meet pipeline gas specifications and emission regulations to ensure production of clean and safe fuel gas to the consumers [5]. Typical pipeline gas specification shown in Table 2 reveals that, for instance, there is a restriction of less than 2% for the composition of CO₂ for natural gas streams to meet delivery specifications for U.S. National Pipeline Grid [6]. Natural gas processing involves mercury removal, sour gas removal, dehydration and separation as shown in Figure 3.

Table 2: U.S. National Pipeline Grid's Natural Gas Composition Specifications for Delivery

Components	Specification
Carbon dioxide	< 2%
Water	< 120 ppm
Hydrogen sulfide	< 4 ppm
C ₃₊ content	950 – 1050 Btu/scf
Dew point	-20oC
Total inert gases (N ₂ , CO ₂ , He, etc)	< 4%

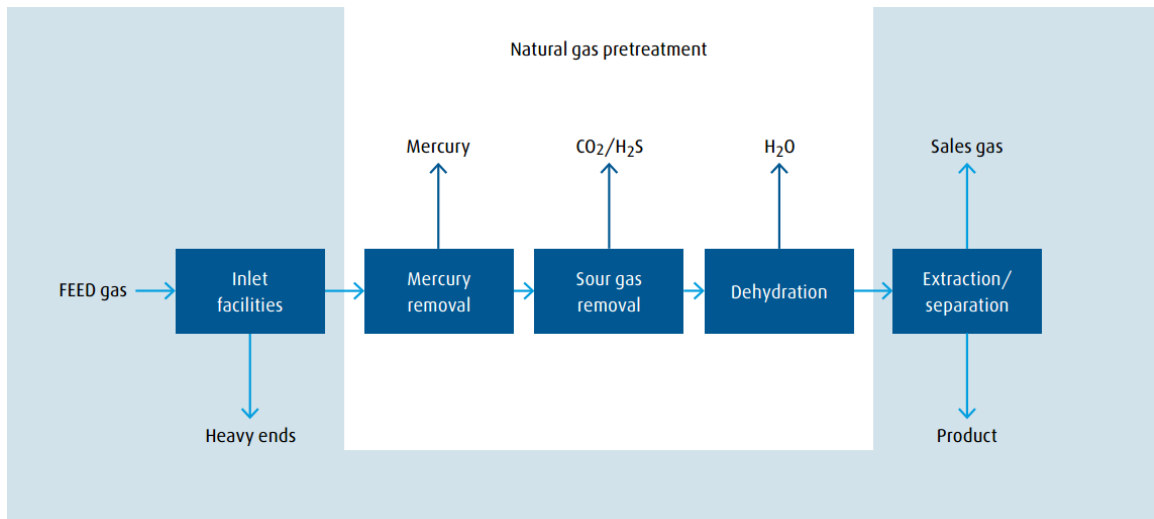


Figure 3: Pretreatment of natural gas

1.3 The need for removal of CO₂

Carbon dioxide is one of the sour gases that need to be removed from natural gas to a level of less than 8% to minimize pipeline corrosion [7]. To meet U.S national Pipeline Grid condition, natural gas should contain less than 2% CO₂ [6] as shown in Table 2. Other drives for CO₂ removal are to meet environmental regulations and to produce more energy efficient fuel.

1.4 CO₂ removal technologies and processes

Several technologies exist for CO₂ removal from natural gas. Major ones include adsorption, absorption, cryogenics and membrane technology.

1.4.1 Absorption

Absorption is the use of solvents for the removal/scrubbing of CO₂. Amine absorption system is a commercially established technology over 60 years ago for CO₂ capture. One of the widely used amine solvents is the Mono-ethanolamine (MEA) which has CO₂ recovery rate of 98% and product purity of 99%. However, some of the challenges associated with this technology include high rate of degradation in oxidizing environment and the large amount of energy involved in the regeneration.

1.4.2 Adsorption

This involves the use of solid sorbents for CO₂ removal from gas mixtures. Common sorbents are zeolites and activated carbon. Two operating modes are possible – Pressure Swing Adsorption and Temperature Swing Adsorption. Gas mixture is passed through bed of sorbents at high pressure for adsorption of CO₂ and regeneration is done at low pressure in the case of pressure swing adsorption while regeneration is done at high temperature for temperature swing adsorption. Major challenges of adsorption include low capacity and low CO₂ selectivity for available sorbents.

1.4.3 Cryogenics

Here, cooling and condensation is employed for the CO₂ separation from gas mixtures. It is a commercially established method used for CO₂ separation from gas mixtures containing high concentration of CO₂. One of the advantages of this method is the direct production of liquid CO₂ which is most times needed for the purpose of transportation. However, one main disadvantage is the large amount of energy requirement for refrigeration for the process.

1.4.4 Membrane Gas separation

Gas separation is one of the membrane processes that is employed for CO₂ separation. Most current gas separations use dense polymer membranes whose permeation mechanism is solution-diffusion as shown in Figure 4**Error! Reference source not found.** [8], [9].

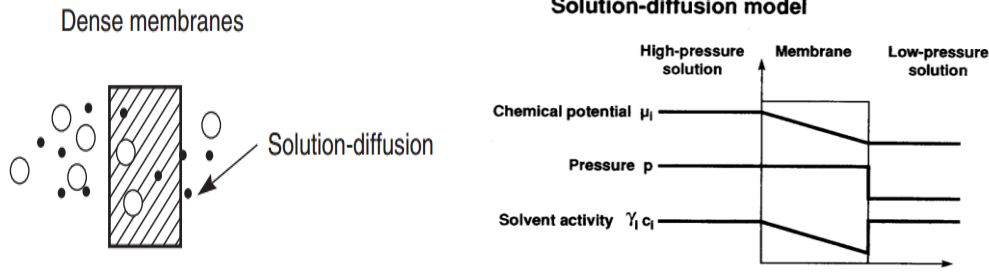


Figure 4: Solution diffusion mechanism of dense membrane.

Transport properties of gas in dense membrane are governed by the expression [9]:

$$j_i = \frac{D_i K_i (p_{i0} - p_{i1})}{l} \quad (1.1)$$

$$\alpha_{ij} = \frac{P_i}{P_j} \quad (1.2)$$

where p_{i0} and p_{i1} are the partial pressures on either side of the membrane, l is the thickness of the membrane, $P_i = D_i K_i$ is the membrane permeability for component i and α_{ij} is the membrane selectivity.

Most gas separation processes using polymeric membrane require extremely thin selective layer in order to achieve high flux. However, most of these membranes are very prone to defects. The effect of defects is eliminated by coating membrane with silicone rubber which is permeable and not selective; and also serves as a protective layer as well.

Membrane materials are generally classified into organic, inorganic and hybrid/mixed matrix membranes. Organic membrane materials are usually polymeric materials such as

polysulfone, polyimide etc which are easy to process. Inorganic membrane materials possess superior separation performance, thermal and chemical stability than polymeric membranes and they are broadly categorized into ceramic materials, glass materials, metallic materials and zeolitic materials [10].

1.5 Advantages of membrane system

Membrane systems possess some major advantages over traditional methods of removing acid gas from natural gas [11].

1. Lower capital cost: Membrane systems are installed as skids, thereby reducing installation cost and it requires no additional facilities.
2. Lower operating cost: The cost of membrane replacement is significantly lower than solvent replacement and energy cost required for one-stage membrane process while the energy requirement for multistage process is comparable to those of the traditional technologies.
3. Operational simplicity and high reliability
4. Good compatibility in terms of space and weight
5. Adaptability
6. Design efficiency
7. Environmentally friendly: Membrane systems do not require handling of spent solvents or adsorbents.
8. Ideal for remote locations

1.6 Performance requirements for membrane materials

The objective of designing membrane materials for several applications is to have high productivity, high selectivity and high durability.

The productivity of membrane material depends on the intrinsic property and geometrical properties of the material. Permeability of the material – an intrinsic property – increases productivity. Productivity also increases with the membrane area exposed for permeation. However, a thin membrane or a thin selective layer is required for better productivity.

Good membrane module design should generally have the following features with the first two being the most critical [12].

1. High area packing density
2. Cost effective manufacturing
3. Low pressure drops on the feed and permeate sides
4. Good flow distribution and flow pattern
5. Minimal concentration polarization

1.7 Mixed matrix membrane

Mixed matrix membranes combine the ease of processability of polymeric membranes with the superior separation properties of inorganic materials. Polymer is the continuous

phase while the inorganic material acts as the discrete phase. Some of the inorganic materials used include zeolite, ceramic etc [9].

Due to the synergistic effect of mixed matrix membrane, the aim of this research is to develop mixed matrix membrane containing carbide derived carbon and polysulfone that will have high CO₂ selectivity with respect to CH₄ for application in natural gas processing.

1.8 Carbide derived carbon (CDC)

CDC is a type of carbon-based nanomaterials (CNM). Other common types include CNTs, graphene, graphene oxide (GO), carbon nanofibers (CNFs), MXene and fullerene [13]. Carbon-based nanomaterials (CNM) generally have unique characteristics such as high chemical, thermal and mechanical strength, conductivity and optical properties. Based on these general properties and other specific characteristics, several researches are currently being conducted to use carbon-based nanomaterials for several applications in many fields including microelectronics, biomedical field and membrane.

The term CDC was coined for carbons produced by the chlorination of inorganic carbides to distinguish them from carbons of organic source [14]. CDCs are pure carbon materials that are derived from carbide precursors by certain synthesis methods such as thermal decomposition, hydrothermal decomposition, and halogenation among others [15]. Common precursors from which CDCs have been produced include TiC, SiC, B₄C [16], ZrC [17], Ti₃SiC₂ and Ti₂AlC etc while Titanium carbide (TiC) remains one of the most

widely used carbides [18]. Different forms of structures of CDC were reported in the literature. A study reveals the structure of TiC-CDC obtained by chlorination to be a disordered amorphous onion-like one [19]. Also, depending on process parameters and location within the CDC film, CDC can contain turbostratic and amorphous carbons, spherical, polyhedral and tubular structures, graphite or diamond [20]. In addition, they can be produced in different forms: as a powder, coating, or membrane [21]

CDCs have desirable properties which have made them good nanomaterial candidate for many applications. They are nanoporous with tunable pore size. Torop et al. [22] reported CDC that was used in his work to have specific surface area $S_{\text{(BET)}}$ 1843 m^2/g , total volume of pores $V_{\text{tot}} = 0.94 \text{ cm}^3/\text{g}$, volume of micropores $V_{\text{micro}} = 0.72 \text{ cm}^3/\text{g}$ and average pore size $\text{APS} = 1.02 \text{ nm}$. Also, Vanadium carbide VC-CDC obtained by chlorination at 900°C , was reported to have pores of an average diameter of 1.18 nm [23]. B_4C -CDC demonstrated high specific surface area close to 2000 m^2/g (for argon adsorption) at the moderately low chlorination temperature of 800–900 $^\circ\text{C}$ [16]. According to Presser et al., [15], a high bulk porosity ($> 50 \text{ vol}\%$) with a high specific surface area (SSA more than 2000 m^2/g) is characteristic of CDC obtained via. CDCs activated with CO_2 or KOH possess distinct improvements in porosity, displaying specific surface areas above 3000 m^2/g and pore volumes above $1.3 \text{ cm}^3 \text{ g}^{-1}$ [24]. According to [21], CDCs have a comparable pore-size distribution with zeolites but a narrower pore-size distribution when compared with single-wall carbon nanotubes and activated carbon. However, many of these properties vary and depend on precursor type, synthesis methods, among others. It was shown by Presser et al. [15] that the structure, pore size, pore size distribution PSD, and specific surface area SSA of the CDC depend

on precursor, halogenation temperatures and post-synthesis annealing. It was also demonstrated in a study done by Gogotsi et al. [21] that the porosity of carbide-derived carbons (CDCs) can be tuned with subångström accuracy in a wide range by controlling the chlorination temperature.

Based on these and other desirable characteristics including their tunability, carbon structure and remarkable volumetric capacitance, CDCs have found applications in many fields. They find applications in gas storage, adsorbents, battery electrodes, molecular sieves, catalysts, supercapacitors for energy storage, water/air filters and medical devices [15, 21, 23]. Specifically, research is expanding towards the use of CDC to develop actuators for electrochemical capacitor applications owing to its remarkable volumetric capacitance and tunable pore size distribution [22]. Methane storage [24] and hydrogen storage [25, 26] with CDCs are also being investigated due to their sorption capacity for these gases.

Specifically for membrane fields, CDC is gaining good research interest for applications in desalination and gas separation. Self-supporting mesoporous silicon CDC was investigated by Porada et al. [27] for capacitive distillation in which a range of carbons were evaluated for capacitive deionization of water. Raka [28] incorporated a novel carbon nanoparticle in polysulfone hollow fiber mixed matrix ultrafiltration membrane for adsorptive removal of benzene, phenol and toluene from aqueous solution for application of treatment of industrial effluent.

In this study, the application of CDC in gas membranes is intended. First, CNT and some other similar carbon materials have been incorporated in membranes for gas separation

application. Furthermore, CDCs have been investigated to be good for CO₂ adsorption. Shahtalebi et al. [29] discovered experimentally that virgin Silicon CDC sample exhibits a relatively high CO₂ adsorption capacity at 273 K (when compared to fluorinated SCDC) and the good performance was attributed to the high porosity of samples, characterized by their large specific surface area and pore volume. Porous carbon materials are doped in order to enhance their CO₂ adsorption. It was summed up in the work of Hong et al. [30] that porous carbon produced at 800 °C from polyvinylidene fluoride (PVDF) exhibited maximum CO₂ adsorption capacities as well good CO₂/N₂ selectivity, with CO₂ adsorption capacity highly depending on the volume of the narrow micropores with size below 0.70 nm, and independent of the specific surface area or pore volume of larger pores. Sulfur-doped nanoporous carbon was evaluated for CO₂ adsorption. Strongly, an inorganic TiC-CDC membrane fabricated as a thin film on macroporous ceramic substrate was tested to possess nitrogen permeability values of 67 Barrer [31]. However, to the best of our knowledge, this is the first attempt to incorporate CDC in mixed matrix membrane for gas separation application.

The objective of this study is to investigate the potential use of CDC in gas membrane especially separation of CO₂ from natural gas. The effect of incorporating CDC in a PSF-based mixed matrix membrane is studied. Also, the effect of temperature on the performance of PSF-CDC mixed matrix membrane is evaluated. Specifically, the CDC used in this research was synthesized from TiC using chlorine treatment synthesis approach. It is expected that the high surface area of CDC will have some positive effects on the separation performance of polymeric membranes. Polysulfone has been chosen as a matrix polymer due to its easy availability and it has been highly investigated. For

instance, the intrinsic CO₂/CH₄ separation performance of pure polysulfone membrane is known and has been reported as a standard [32]. Also, low cost, good gas separation properties and widespread use as commercial polymer make it a good candidate for our research. In addition, a type of carbon nanoparticles has been successfully incorporated in PSF-based mixed matrix membrane however for ultrafiltration application in the treatment of industrial wastewater [28].

Table 3: Intrinsic permeation properties of polysulfone

Permeability coefficient (Barrer)		Intrinsic selectivity
CO ₂	CH ₄	CO ₂ /CH ₄
4.5	0.16	28.1

$$1\text{Barrer} = 10^{-10} [\text{cm}^3(\text{STP}) \text{ cm} / \text{cm}^2\text{s cmHg}]$$

1.9 Research objectives

The main objective of this MSc research is to test the potential of carbide derived carbon in polysulfone-based mixed matrix membrane for the application of CO₂ separation from natural gas. The detailed objectives include:

- 1) Preparation of pure polysulfone and Polysulfone/CDC mixed matrix membrane with appropriate post treatment.
- 2) Characterization of the prepared membranes with different advanced characterization techniques such as Scanning Electron Microscopy (SEM), FTIR, XRD, and Thermogravimetric analysis (TGA).

3) Testing of the membrane for CO₂/CH₄ separation using the lag time method (constant volume method). The effects of parameters such as feed pressure, operating temperature, CDC loading on the separation performance of the mixed matrix membrane are extensively studied and optimum parameters shall be reached

CHAPTER 2

LITERATURE REVIEW

2.1 Introduction to gas membranes

Highly efficient gas separations can be achieved by using membranes which predominantly function based on the solution-diffusion mechanism. The structures of different type of gas membranes are illustrated by Figure 5. Asymmetric membranes consist of dense top layer and porous under layer. Generally, the most basic and important requirements which gas membranes should satisfy are high permeability and high selectivity; other requirements include manufacturing reproducibility, long term stability under high feed pressure, economical manufacturing process, chemical and thermal stability. The high flux and selectivity of membranes drive its economic competitiveness with other separation technologies. This is because the higher the selectivity, the lower the driving force and consequently the lower the operating cost. Similarly, the higher the permeation rate, the smaller the required membrane area and therefore the lower the capital cost of the membrane.

Furthermore, for an ideal gas membrane, the selective layer should be defect-free and thin to maximize gas flux. Similarly, the supporting substructure should be strong enough to provide mechanical support for the selective layer but it should not contribute to the resistance of the gas transport through the membrane.

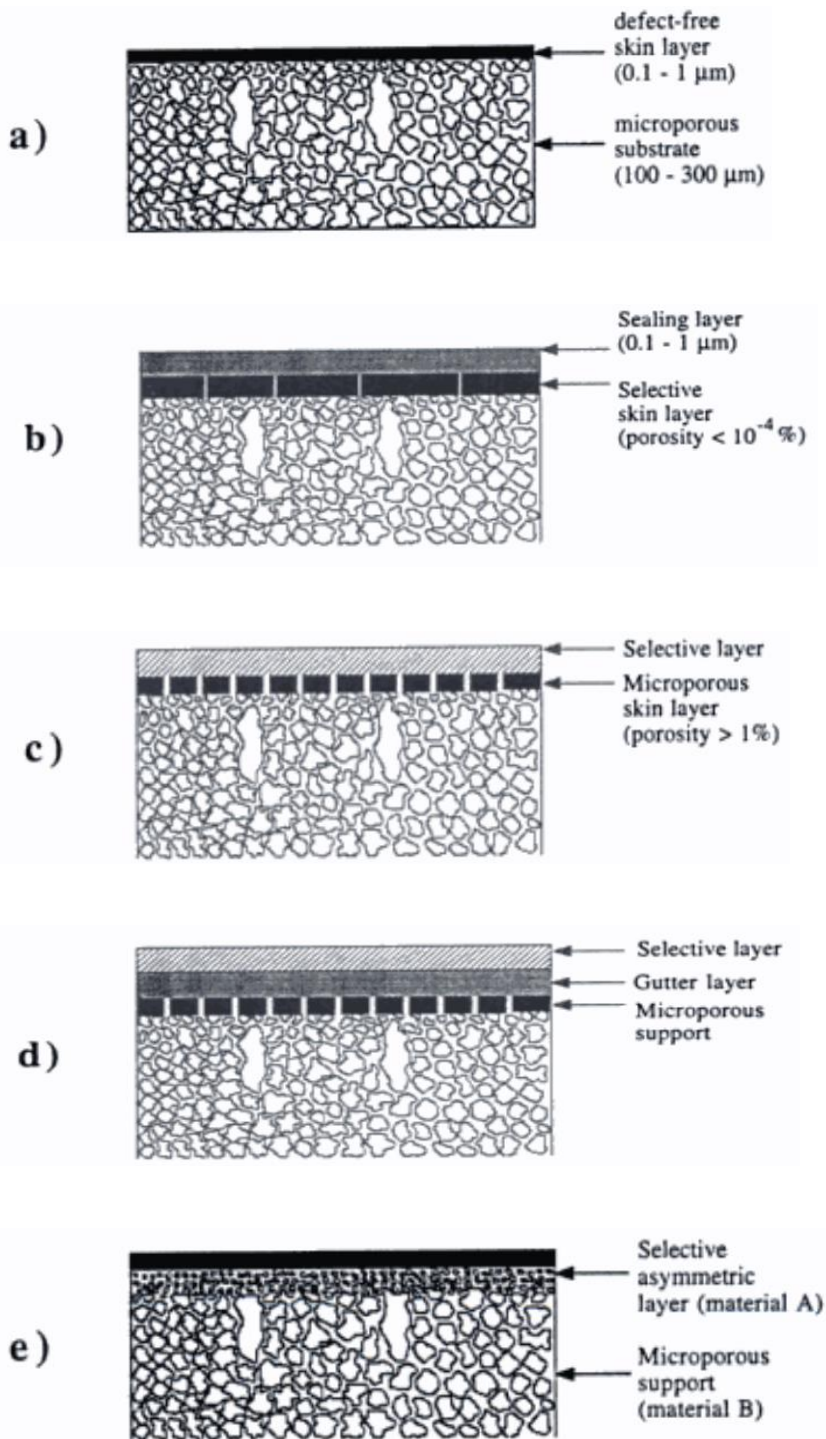


Figure 5: Structures of gas separation membranes (a) integrally skinned asymmetric; (b) multicomponent ('cauked'); (c) single layer thin-film composite; (d) multilayer thin-film composite; (e) asymmetric composite.

2.2 Gas membrane formation

The phase inversion remains one of the common methods of producing membrane materials which can be used for gas separation. They can be categorized into three: wet phase inversion, dry phase inversion and the dry/wet phase inversion.

2.2.1 Wet phase inversion

This technique involves casting a homogeneous solution consisting of polymer and solvents on a support or glass plate and allowing a partial evaporation of solvents from the surface of the membrane prior to immersion of the forming membrane in coagulation bath. Common coagulants include water bath, ethanol, methanol and few other non-solvents. The partial solvents evaporation during the wet phase inversion is optional and its importance has been suggested by some researchers [33].

Generally speaking, membranes produced by wet phase inversion technique have been reported to have too many defects which limit their use for gas separation applications.

2.2.2 Dry phase inversion

In this technique, the cast membrane is left for drying without immersion in coagulation bath. Therefore, the membrane formation is caused by the sole removal of the solvent and non-solvent component by evaporation. After complete solvent and non-solvent removal, a dense homogeneous film is formed [12].

2.2.3 Dry/wet Phase inversion

In this technique, the casting solution usually consists of carefully selected ratio of solvents and non-solvents in addition to the polymer. Immediately after casting, the forming membranes are allowed to undergo the dry phase step which involves allowing the membrane for a defined period of time for loss of volatile solvent. After this, the nascent membrane is then immersed in coagulants for the wet phase step.

The use of two solvents in addition to non-solvents allows a finer control of solvent evaporation and this is important in the formation of the top dense layer of the asymmetric membrane. However, the two solvents and non-solvents should be miscible with themselves and with the coagulation bath. Usually, THF is commonly used as the volatile solvents for phase inversions involving water coagulations. Also, common non-volatile solvents in water coagulation process include NMP, DMAC, DMF among others. Aliphatic alcohols such as ethanol and propanol are used as non-solvents [33]. This technique is known for the production of integrally skinned asymmetric membranes which are used for gas separation.

The three types of inversion techniques are described by Figure 6.

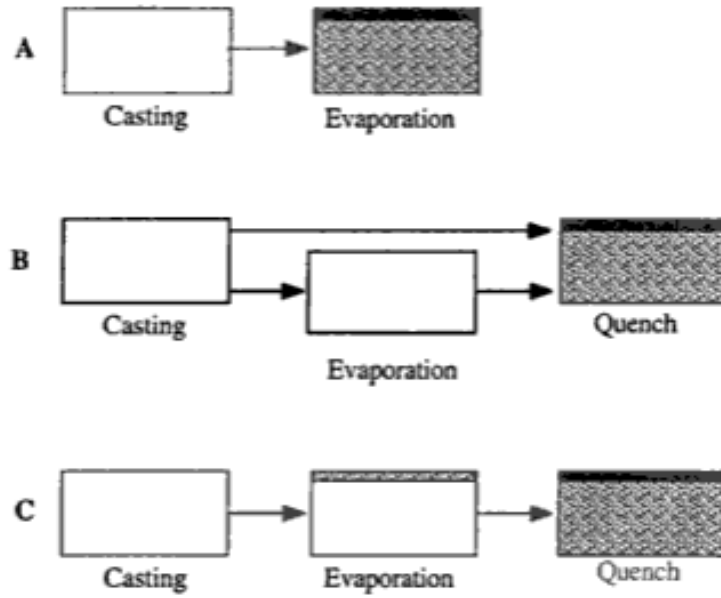


Figure 6: Schematic representation of phase inversion techniques - (a) dry phase inversion (b) wet phase inversion (c) dry/wet phase inversion

2.3 Fundamentals of Gas separation membranes

The transport through gas membrane is studied by using the solution-diffusion model.

For a single gas, the transport follows the Fick's law:

$$J = -D \frac{dc}{dx} \quad (2.1)$$

J is the gas flux, dc/dx is the concentration gradient and D is the diffusivity. By further analysis, the above expression becomes

$$J = \frac{SD}{l} \cdot \Delta p \quad (2.2)$$

Where l is the membrane thickness and Δp is the transmembrane pressure difference.

Permeability is defined as

$$P = S \cdot D \quad (2.3)$$

Therefore,

$$J = \frac{P}{l} \cdot \Delta p \quad (2.4)$$

In case membrane thickness cannot be measured, P/l also known as the permeance is measured instead of the permeability.

2.4 Commercial membrane and membrane processes

The vast majority of membranes used commercially are polymer-based. Some of membrane processes are developed while others are developing. Microfiltration, ultrafiltration, reverse osmosis and electrodialysis are well established membrane processes whose separation technologies have been developed for industrial application. Gas separation and Pervaporation are developing industrial membrane separation technologies for industrial application with a number of installed plants and expanding markets. Membrane-based gas separation systems are offered by companies for separation of hydrogen from nitrogen, CO₂ from natural gas etc. [9]

2.5 Mixed matrix membrane for CO₂ separation

Mixed matrix membranes have become trending option for the application of membrane technology to CO₂ separation from natural gas as a result of their advantages over polymeric membranes. Many researchers have delved into this area and lots of different inorganic materials have been incorporated into various polymers. Separation performances of polymeric membranes have been reported to be greatly enhanced as a result of incorporation of inorganic fillers in these membranes. Some inorganic materials incorporated in polymers were reviewed and are being reported here. These materials include MOFs, ZIFs, Magnesium oxide (MgO), Titanium oxide (TiO₂), Carbon-silica material (CSM), Aluminium oxide (Al₂O₃).

The effects of structural parameters such as NH₂-functionalized MIL-type MOFs loading and membrane thickness as well as those of operational variables on the Polysulfone (PSF) and Polyimide (PI) MMM were compared by Rodenas et al. [11]. It was found out that PI-based membrane generally showed superior separation performance than PSF-based membrane.

Membrane synthesis method is one of the key parameters to be optimized to achieve a good separation performance for mixed matrix membrane. Waqas et al. [12] explored this concept by synthesizing a well-optimized mixed matrix membrane of polyimide matrix containing amine-functionalized MIL-125(Ti) MOF at different loading up to 30 wt% and measuring its separation performance against that of MMM of the same polymer matrix containing ordinary MIL-125(Ti) MOF at the same loading range. It was discovered that the carefully tuned membrane synthesis method has some positive effects

on the CO₂ separation performance of the membrane. A mixed gas CO₂:CH₄ (50:50) permeation performance evaluation of the MMMs revealed that an optimal selectivity of 50 was achieved at 15wt% loading while an optimal CO₂ permeability of 50 was achieved at 30 wt% loading for the amine-functionalized MIL-125 fillers MMM at 9 bar pressure. Furthermore, based on comparison with other previous work, it was shown that the amine-functionalized MIL-125 fillers MMM of polyimide matrix is superior to polysulfone-based mixed matrix membrane containing the same filler; with a 550% increased selectivity and 35% increased CO₂ permeability .

Generally, separation performance of mixed matrix membrane is expected to be significantly influenced by the particle size of fillers. Nordin et al. [13] investigated a simultaneous influence of particle size of ZIF-8 together with heat treatment on the CO₂/CH₄ separation performance of polysulfone/ZIF-8 mixed matrix membrane, in which ZIF-8 of different particle sizes was achieved by using different concentrations of the base-type triethylamine (TEA) additive during synthesis. It was shown that dispersing smaller ZIF-8 particles in polysulfone resulted into a decreased permeance and increased selectivity while heat treatment of ZIF-8 resulted into increased permeance and decreased selectivity, and also with the effects of particle size was discovered to be more for the heat-treated ZIF-8 mixed matrix membranes than the as-synthesized ZIF-8 MMM. Partial pore blockage for small pores was attributed to hindered CH₄ permeation and hence enhanced CO₂/CH₄ selectivity of 28, and the heat treatment is believed to evacuate any guest molecules from the pores thereby leading to increased unselective permeability. However, Chi et al. [14] made a systematic investigation of the sole effect of only particle size of ZIF-8 on CO₂ gas separation performance of polystyrene-block-

poly(ethylene-ran-butylene)-block-polystyrene (SEBS) copolymers/ZIF-8 mixed matrix membrane. Three (3) different sizes of ZIF-8: ZIF-8(S), ZIF-8(M) and ZIF-8(L) of sizes 88, 240 and 533 nm were synthesized using the precursors zinc nitrate, zinc acetate and zinc chloride respectively with methanol due to its easy removal and weak interaction with ZIF-8, but all the synthesized particles have similar pore structures and surface areas as confirmed by appropriate characterizations. Time-lag method gas permeation in which pure gases are injected at low pressure (100 Torr, far less than atmospheric pressure) with the downstream at much lower pressure (2 Torr) to simulate mixed gas permeation case, was used to evaluate and compare the performance of the neat SEBS membrane and SEBS/ZIF-8 mixed matrix membrane. Some enhancement in gas permeability as a result of incorporation of ZIF-8 regardless of size was observed, however the mixed membrane formed by the incorporation of 30 wt% ZIF-8 (M) of size 240 nm appeared to be the most effective in terms of separation performance with CO₂ permeability of 454.6 barrer corresponding to a 2.5 fold increase from that of neat SEBS membrane, and a selectivity of 5.4 also at 30 wt% filler loading. The low performance behavior of SEBS/ZIF-8(L) could be attributed to hindered CO₂ permeation as a result of high mass transfer resistance at enhanced sites while reduced interfacial contact area was said to be responsible for increased unselective permeability.

The incorporation of hollow MOF spheres including ZIF-8 spheres in polymer matrix to fabricate mixed matrix membrane is rarely reported in the literature; however, S. Hwang et al [15] recently reported some work in this area, in which low density hollow ZIF-8 (H_ ZIF-8) spheres were synthesized in a two-step process: solvothermal surface coating of polystyrene cores with ZIF-8 shells and selective removal of the PS core with DMF

solvent. Consequently, the synthesized spheres were dispersed (from 0, 10, 20 to 30 wt%) as inorganic fillers in amphiphilic graft copolymer poly(vinyl chloride)-g-poly(oxyethylene methacrylate) (PVC-g-POEM) synthesized by atomic transfer radical polymerization (ATRP) to prepare defect-free, free-standing mixed matrix membrane via solution casting method. A time-lag method of gas permeation measurement was employed to investigate the influence of the hollow ZIF-8 loading on the membrane separation performance and it was found out that there is an enhancement in the gas permeation as a result of the introduced hollow ZIF-8 particles. For instance, it was shown that dispersion of 30 wt% of hollow ZIF-8 led to a high CO₂ permeability of 623.0 Barrer, corresponding to about 8.9-fold increase from permeability in neat PVC-g-POEM membrane although with a slight reduction in selectivity from 13.7 to 11.2.

Filler dispersion leading to improved interaction between polymer and fillers is one of the parameters that can be tuned to optimize the separation performance of mixed matrix membrane. Having control over dispersion of fillers gives the opportunity to increase filler content in mixed matrix membrane with acceptable or no occurrence of defects. Several reports in the literature have been recorded about certain attempts to improve polymer-filler interaction. S. Shahid et al.[12] reported a novel way to prepare super-performing polymer/MOF mixed matrix membrane with polyimide/MOF as a case study.

Farhan and Rizafizah [16] studied the effect of MgO filler in a (60:40 w/w %) Epoxidized Natural Rubber (ENR)/ Polyvinyl Chloride (PVC) polymer matrix on CO₂ permeation. As reported by different authors, PVC was investigated to provide mechanical strength for the membrane while ENR-50 provides flexibility and mechanical

toughness for a self-supporting membrane. The percentage of filler in the matrix was limited to 8% to avoid filler agglomeration and membrane brittleness. Gas permeation tests with purified CO₂ and purified N₂ at pressures of 2, 4 and 6 bars and room temperature showed that the permeabilities of CO₂ and N₂ at 6 bar in 8% MgO filled MMM are 40000 and 27000 barrers respectively. The high permeation of CO₂ was attributed to its smaller kinetic size and its interaction with the MgO fillers due to the acidity nature of CO₂.

The incorporation of amine-functionalized TiO₂ submicrospheres into Sulfonated poly(ether ether ketone) (SPEEK) was investigated by Qingping et al [17]. The SPEEK used for the study was at 67% degree of sulfonation and the TiO₂ submicrospheres used were functionalized with dopamine (DA) and polyethyleneimine (PEI) in succession. It was observed that humidification of the MMM enhanced CO₂ separation performance (both permeability and selectivity) due to enhanced solubility of CO₂ through acid-base interactions. A significantly higher separation performance than SPEEK/TiO₂ and SPEEK/TiO₂-DA was recorded for SPEEK/TiO₂-DA-PEI as it was shown that at 15 wt % loading, the ideal CO₂/CH₄ selectivity and the ideal CO₂/N₂ selectivity increased from their corresponding values for pure SPEEK membrane by 102% and 65% to 58 and 64 for SPEEK/TiO₂-DA-PEI membrane respectively, with a CO₂ permeability of 1629 Barrer at 1 bar and 25 C.

Qingping et al. [18] made further investigations on mixed matrix membranes for CO₂ separation by synthesizing one-dimensional animated titania nanotubes (TNT-IM) and incorporating them into SPEEK of 69% degree of sulfonation. The pure titania nanotubes were (TNT) prepared by hydrothermal reaction from TiO₂ and were subsequently

modified accordingly by 3-(methacryloxy) propyltrimethoxysilane (MPS) and 1-vinylimidazole (IM) to form the TNT-IM filler. It was shown that SPEEK/TNT-IM membrane exhibited the highest selectivities of 56.8 and 62.0 for CO₂/CH₄ and CO₂/N₂ systems, respectively, with a CO₂ permeability of 2090 Barrer at 25 °C and 1 bar. The increased permeability and selectivity were explained to be mainly as a result of large aspect ratios (length/width) and abundant amine groups from aminated titania nanotubes as well as the good polymer-nanotube interfacial compatibility [3].

Based on the two recent works done by the research group of Qingping et al. [18] on SPEEK-based MMM, it can be observed that SPEEK-based MMM with aminated titania nanotubes (TNT-IM) may give better CO₂ separation performance than the MMM doped with TiO₂-DA-PEI.

The potential of porous Carbon-Silica Nanocomposite Material CSM for mixed matrix membrane for CO₂ separation was investigated by M. Waqas Anjum et al [19]. CSM-18.4 and CSM-23.3 fillers containing 18.4 and 23.3 wt% of carbon, respectively were prepared via MCM-41 by incipient wetness impregnation. The MCM-41 and the CSMs were differently incorporated into polyimide (PI) and it was shown that the separation performance of the CSM-based MMMs is significantly higher than those of MCM-based MMM and unfilled PI. For gas mixtures with a 50:50 (CO₂:N₂) feed composition, mixed gas selectivity (up to 42.5) and permeability (up to 27 Barrer) increased by 2-fold and 6-fold respectively when compared to the performance of unfilled PI [20].

Shadi et al. [21] carried out a study of the influence of certain various silica nanoparticles in polyesterurethane (PU) mixed matrix membranes (MMM) on the

transport behaviours of CO₂ and CH₄. Non-modified and commercially-modified silica (with octylsilane and polydimethylsiloxane) were used as fillers to form PU/silica-Un, PU/silica-Os and PU/silica-PDMS MMM. Gas permeation results showed that CO₂ permeability is significantly higher than that of CH₄ in pure PU membrane and silica filled PU MMM, due to its low kinetic diameter, higher condensability and better interaction with the polar groups of the polymer [5]. The results revealed that among silica nanoparticles, unmodified silica showed better performance for CO₂ /CH₄ separation [21].

The influence of alumina nano-particles on CO₂ /CH₄ separation performance criteria of poly(4-methyl-1-pentyne) known as TPX was evaluated by Mohammad et al. in their research [22]. Mixed matrix membranes (MMMs) containing different weight percent of alumina nano-particles were prepared by solution casting method. The gas permeation results revealed that gas permeability as well as CO₂/CH₄ selectivity increased with increasing alumina loading in TPX matrix. At the operating condition of 8 bar pressure, the CO₂ permeability increased significantly from 157.43 Barrer at no embedded TPX to 527.78 Barrer in TPX loaded with 30 wt% of alumina. The CO₂ /CH₄ selectivity in 30 wt% alumina loaded TPX was obtained to be 12.51 compared to the 7.73 value in pure TPX. Review summary of some of the literature reviewed is as shown in Table 4.

Mixed matrix membrane containing PSF and carbon nano-fibers CNF fabricated using NMP solvents, and tested was reported in the work of Dehghani et al [34]. Morphology investigation of the mixed matrix membranes through SEM pictures showed that only few agglomerations as a result of intermolecular force were observed in the 1 wt% PSF/CNF and hence the study was limited to the maximum of 1 wt% loading of the CNF.

Surface roughness was also observed to increase with increasing loading as shown through the Atomic force microscopy images and the increasing calculated surface roughness parameters. Permeation tests of these membranes at 4 bar feed pressure and room temperature, using the constant pressure method, showed that the mixed matrix membrane exhibited high permeability as CNFs/PSF membrane permeability raised from 0.71 to 4.87 Barrer for CO₂ with increasing concentration of CNF while CH₄ permeability was similarly found to increase with loading. Increased gas permeability by incorporating CNF was justified based on its large diameter of 100 nm (significantly larger than CO₂ and CH₄ size of 0.34 and 0.38 nm respectively) and good interaction between the polymer phase and CNF surface. Also, the possibility of the CNF orienting in the vertical direction and consequently causing pinholes on membrane surface was not overlooked. Furthermore, CO₂/CH₄ selectivity was found to increase with increasing CNF loading to maximum selectivity of 12.17 at 1 wt% CNF loading, for 4 bar feed gas and room temperature testing. The polar carboxyl group on the CNF, confirmed by FTIR has stronger interaction with polar gas, such as CO₂ and O₂, than non-polar gas and this is believed to have played a significant role in the selectivity hike. Here, the obtained performance could be based on the compromise between the positive effect of chemical composition of the CNF and the negative impact of its size and shape on separation factor of the mixed matrix membrane.

In a study to investigate the mode of gas transport and general trends in nonporous nanosized silica/low-free-volume glassy polymers, chloroform-prepared PSF/silica mixed matrix membrane was tested for gas separation by Ahn et al. [35]. Contrary to the prediction of Maxwell model for nonporous filler membrane, the gas permeabilities

including those of CH₄ and CO₂ for silica-filled PSF were higher than those of unfilled PSf and increase as the volume fraction increases. Therefore, instead of the fumed nonporous silica to cause decreased diffusivity due to increased tortuosity in the polymer matrix as predicted by Maxwell theory, it is believed to have caused disruption of polymer chain packing which leads to increased free volume and consequently increased diffusivity. In addition, an increase in agglomerate size with silica content shown by TEM and SEM images, results in an increase in void size of the PSF-silica interface, eventually leading to permeability enhancement. Unexpectedly, gases such as CH₄ are found to witness more permeability enhancement by incorporating silica than smaller gas such as CO₂. It is assumed that the effect of increasing free volume size due to the introduction of fumed silica is more directed towards the small cavities in the low-free-volume PSf and thus larger penetrants such as methane, which have low permeability in the low-free-volume PSf, have a larger relative permeability enhancement than smaller gases such as oxygen. As a result of this, a decrease in ideal selectivity for O₂/N₂ and CO₂/CH₄ with the silica loadings in PSf/silica MMMs was obtained.

Table 4 summarizes the performances of some of the mixed matrix membranes developed for CO₂/CH₄ separation.

Table 4: Review summary

polymer	Filler	P (bar)	T (K)	Permeability of CO2 in (Barrers)	Selectivity= Perm(CO2)/Perm.(CH4)	Loading (% filler)	Reference
Polydimethylsiloxane (PDMS)	p-KIT Silica	0.5	308	12 × 10 ³ Barrer	1.92 (CO2/N2)	2 wt%	[23]
Polyurethane (PU)	Silica nanoparticle (Unmodified)	10	299	12.03 barrer	25	15 wt%	[21]
Sulfonated poly(ether ether ketone) (SPEEK)	Aminated Titania Nanotube (TNT-IM)	1	298	2090 barrer	56.8 (Ideal selectivity)	8 %	[18]
Epoxidized Natural Rubber (ENR)/ PVC	MgO	6	298	40,000 barrers for pure CO2 permeation	1.4 (CO2/N2)	8 %	[16]
Polyimide	Carbon-Silica Nanocomposite Material (CSM)	1	298	27 barrer	mixed gas selectivity up to 42.5 CO2/N2		[20].
Sulfonated poly(ether ether ketone) (SPEEK) with 67% degree of sulfonation	Amine-functionalized TiO2 submicrospheres;	1	298	1629 barrer	58 (Ideal selectivity)	15 %	[17]

PSF	CNF	6	298	5.4	16.41	1 wt%	[34]
PSF	Fumed silica	4.4 at m	35 C	6.3 – 19.7	18 - 29	0 - 0.20 volume fraction	
PSF	CNF			12	12.2		[34]
PSF	NH ₂ -MIL-53(Al) MOF			6	46		[36]

CHAPTER 3

METHODOLOGY

This chapter discusses some of the experimental procedures for this work. Overall, the experimental work includes membrane preparation, characterization and testing.

3.1 Materials

Polysulfone pellets ($M_w \sim 35,000$) also termed as PSF in this work, 1-Methyl-2-pyrrolidinone (NMP), tetrahydrofuran (THF), Polydimethylsiloxane (PDMS) and n-hexane used for the preparation of membranes were purchased from Sigma Aldrich while ethanol was supplied by Merck. CDC used in this study was synthesized by our group from TiC with the following features: microporous structure with narrow pore size distribution, BET surface area of $2589 \text{ m}^2/\text{g}$ and a total pore volume of 1.26 cc/g [37]. Deionized water was used for all water processes.

3.2 Membrane Preparation

Pure and mixed matrix membrane samples were prepared using the solution-casting method with a dry/wet phase inversion for solvent exchange. Procedure is similar but not exactly the same as that reported in the work reported by Nordin [38]. Casting solution

of pure sample was made of PSF in a mixed solvents of NMP (45 wt%), THF (15 wt%) and ethanol (10 wt%). Mixed matrix membrane samples contained, in addition, different amounts of CDC, with CDC loading computed according to:

$$CDC \text{ loading } (\%) = \frac{\text{mass of CDC (g)}}{\text{mass of CDC (g)} + \text{mass of PSF (g)}} \times 100\% \quad (3.1)$$

Both the CDC and PSF pellets were firstly vacuum-dried at 100 °C overnight to remove absorbed moisture. Appropriate amount of CDC particle was added to a solvent mixure of NMP/THF/Ethanol and consequently dispersed for 30 minutes by sonication. Right amount of PSF was then added and kept stirring for 24 hrs to ensure total dissolution and good homogeneity. The resulting solution was degassed for 30 minutes to remove gas bubbles. The amount of gas bubbles and consequently the degassing time were small because the stirring was done at low rpm. The prepared solution was then casted on a glass plate using casting knife at a uniform thickness of 200 microm. A free standing evaporation period of 60 secs was allowed before the casted film was immersed in water bath for 24 hrs for solvent exchange. Pure samples were prepared with the omission of addition of CDC and hence sonication. Membrane samples were consequently dried at ambient conditions for a day. Surfaces of the prepared membrane samples were coated with 10 wt% PDMS in n-hexane by dip coating method followed by curing at 100C for about 12 hrs. Table 5 shows the compositions of the casting solutions used to prepare all the membranes used in this work.

Table 5: Compositions of casting solutions

S/N	Membrane sample	PSF (wt%)	CDC (wt%)	NMP/THF ratio	Ethanol (wt%)
1	P1	15	0	3/1	10
2	P2	20	0	3/1	10
3	P3	25	0	3/1	10
4	P4	30	0	3/1	10
5	P5	35	0	3/1	10
6	M0.1	30	0.1	3/1	10
7	M0.5	30	0.5	3/1	10
8	M1.0	30	1.0	3/1	10
9	M2.0	30	2.0	3/1	10

3.2.1 Loading Range

The loading of CDC used in this study was carefully determined based on intuition from the literature. Filler loadings in various PSF-based mixed matrix membranes were considered. More importantly, significant consideration was given to the loadings of different carbon materials as fillers in membrane in deciding the range of CDC loading in our membrane. Findings about these are detailed in Table 6

Table 6: Filler loading in mixed matrix membrane

S/N	Polymer	Fillers	Loading tested	Observation/Remark	Ref
1	Polymer of intrinsic microporosity PIM-1	UiO-66 MOFs	0-28 wt%		[39]
2	PSF	rice husk extracted silica	0 – 40 wt%		[40]
3	PSF	carbon nano-fibers (CNF)	0, 0.01, 0.1, 1 wt%	Agglomeration at 1 wt% observed based on SEM images	[34]
4	PSF	SAPO-44 zeolite	5 – 20 wt%	Agglomeration at 10 and 20 wt% from cross section SEM images	[41]
5	PSF/PI	Silica	5 – 20 wt%	Homogeneity up to 15 wt%	[42]
6	PSF	silica nanoparticle	0 – 0.2 vol fraction (0 – 31 wt%)	Agglomeration increases with loading	[35]

7	PSF	Functionalized MOFs	8, 16, 25 and 40 wt%	Homogeneous filler distribution at all loadings	[36]
8	polyimide	Functionalized multi-walled carbon nanotubes	0.5–1 wt%	Optimum loading of 0.7 wt%	[43]
9	PSF	Novel carbon nanoparticle	0, 0.5, 1, 2 and 4 wt%	No pores observed beyond 1 wt%. At higher nanoparticle loading, pores are blocked and the membrane becomes dense.	[28]
10	PSF	Zinc oxide	0.0, 0.1, 1.0, 3.0, and 5.0 wt%		[44]
11	PDMS	CNT	0 – 10 wt%	Agglomeration at 10 wt%	[45]

Because of the problem of filler agglomeration, filler loading is limited by an upper bound. Functionalized multi-walled carbon nanotubes belonging to same carbon material like CDC has an optimum loading of 0.7 wt%, carbon nanofibres a maximum of 1 wt% testing, and a novel carbon particle was tried up to a loading of 4 wt%. Since CDC is a carbon material like these particles, we have decided to try a maximum loading of 2 wt%. Other loadings are 0.1, 0.5 and 1 wt%

3.3 Characterization of membrane samples

Morphologies of the membranes as well as other properties are important to understand the structures of the membrane and their relevance to transport properties of gases through the membrane. The prepared membrane samples were therefore characterized using the following techniques.

3.3.1 Scanning Electron Microscopy

SEM images of membrane surface and cross section were obtained for morphology analysis. The images were taken with TESCAN SEM equipment. Prior to this, membrane samples for cross section analysis were fractured in liquid nitrogen and then coated with gold.

3.3.2 X-ray diffraction

An X-ray diffraction pattern is a plot of the intensity of X-rays scattered at different angles by a sample. The detector moves in a circle around the sample and its position is recorded as the angle 2θ (2θ). It records the number of X-rays observed at each angle 2θ and the X-ray intensity is usually recorded as “counts” or as “counts per second”.

The XRD patterns of CDC, pure and mixed matrix membrane samples were recorded on An XRD equipment. The recorded range of 2θ was $4\text{--}60^\circ$ and the scanning speed was

2°/min for the CDC nanoparticle while the recorded range of 2θ was 4–50° [46] and the scanning speed was 10°/min for the membranes.

3.3.3 Fourier Transform Infrared Spectroscopy (FTIR)

Infrared spectroscopy is a technique that is based on the vibrations of the atoms of molecules. An infrared spectrum is commonly obtained by passing infrared radiation through a sample and determining what fraction of the incident radiation is absorbed at a particular energy. The energy at which any peak in an absorption spectrum appears corresponds to the frequency of a vibration of a part of a sample molecule. For a molecule to show infrared absorptions, it must possess a specific feature, that is, an electric dipole moment of the molecule must change during the vibration. This is the selection rule for infrared spectroscopy. The interactions of infrared radiation with matter may be understood in terms of changes in molecular dipoles associated with vibrations and rotations. A molecule can only absorb radiation when the incoming infrared radiation is of the same frequency as one of the fundamental modes of vibration of the molecule. This means that the vibrational motion of a small part of the molecule is increased while the rest of the molecule is left unaffected. Vibrations can involve either a change in bond length (stretching) or bond angle (bending). Some bonds can stretch in-phase (symmetrical stretching) or out-of-phase (asymmetric stretching).

The mid-infrared spectrum in the range of 4000–400 cm^{-1} makes up four regions whose locations generally determine the nature of a group frequency. Overall, the regions are categorized as follows: the X–H stretching region (4000–2500 cm^{-1}), the triple-bond region (2500–2000 cm^{-1}), the double-bond region (2000–1500 cm^{-1}) and the fingerprint

region (1500–600 cm^{-1}). The fundamental vibrations in the 4000–2500 cm^{-1} region are generally due to O–H (3700–3600 cm^{-1}), C–H (3100–2850 cm^{-1}) and N–H (3400 and 3300 cm^{-1}) stretching. C≡C bonds absorb between 2300 and 2050 cm^{-1} , while the nitrile group (C≡N) occurs between 2300 and 2200 cm^{-1} . The principal bands in the 2000–1500 cm^{-1} region are due to C=C and C=O stretching.

Alkanes contain just C–C and C–H bond and the spectra contains a lot of information.

Alkenes contain the C=C group and the four major bands associated with this molecular fragment are the in-plane and out-of-plane =C–H deformations, =C–H stretching and C=C stretching. Alkynes contain the C≡C group in addition to three other characteristic bands: C≡C stretching, ≡C–H bending and ≡C–H stretching. The characteristic bands of alkanes, alkenes and alkynes are shown in Table 7 **Error! Reference source not found.**

Relevant characteristic infrared bands are exhibited by aromatic compounds in five regions of the mid-infrared spectrum as shown in Table 8.

Fourier transform infrared spectra of membrane samples were measured on a Nicolet 6700 FTIR spectrometer in the range of 400–4000 cm^{-1} , using the KBr method. However, the spectra were further analyzed in different ranges of wavenumber.

Table 7: Aliphatic hydrocarbons characteristic infrared bands

Wavenumber (cm^{-1})	Assignment
	Alkanes
2960	Methyl symmetric C-H stretching
2930	Methylene asymmetric C-H stretching
2870	Methyl asymmetric C-H stretching

2850	Methylene symmetric C-H stretching
1470	Methyl asymmetric C-H bending
1465	Methylene scissoring
1380	Methyl symmetric C-H bending
1305	Methylene wagging
1300	Methylene twisting
720	Methylene rocking
	Alkenes
3100-3000	=C-H stretching
1680-1600	C=C stretching
1400	=C-H in-plane bending
1000-600	=C-H out-plane bending
	Alkynes
3300-3250	=C-H stretching
2260-2100	C≡C stretching
700-600	=C-H bending

Table 8: Aromatic compounds characteristic infrared bands

Wavenumber (cm ⁻¹)	Assignment
3100-3000	=C-H stretching
2000-1700	Overtone and combination bands
1600-1430	C=C stretching
1275-1000	in-plane C-H bending
900-690	Out-of-plane C-H bending

3.3.4 Thermogravimetric analysis (TGA)

TGA Measures changes in weight with respect to changes in temperature. Both weight loss and derivative weight loss curves can be obtained. The weight loss curves give information about changes in sample composition and thermal stability while the derivative weight loss curve can be used to determine the point exhibiting the most apparent weight loss.

Samples were dried at 100 °C in vacuum oven overnight to remove residual solvents. Thermogravimetric analysis (TGA) of pure and mixed matrix membrane samples was performed on a SDT Q600 TA instrument. A certain quantity of sample was placed on the aluminum pan sample holder, equilibrated at 30°C and then heated up at the rate of 10°C min⁻¹ to 800°C [46] under a constant flow of nitrogen gas at 100 ml/min.

3.4 Gas Permeation

Gas permeation properties of the pure and mixed membranes were determined using the constant volume/variable pressure method on the Convergence Inspector Neptunus gas permeation equipment schematically displayed Figure 7. The membranes were mounted in the cell and tested with pure gases in the order of CH₄ and CO₂ at different operating temperatures and feed pressures.

Before carrying out permeation experiments, the whole system especially the downstream section is evacuated in order to remove adsorbed species on membranes and until the downstream pressure is reduced to below 0.1 mbar. During evacuation, the oven

temperature is set such that the desired cell temperature is reached. Leakage is then evaluated for about 10 minutes and the feed is introduced at set pressure. Usually, leakage is found to be in the order of 10^{-8} mbar/sec. Permeation through the membrane is monitored by the increase in downstream pressure with time. The curve is analyzed and gas permeability is obtained according to:

$$P = \frac{V_d l}{P_2 A R T} \left[\left(\frac{dP_1}{dt} \right)_{ss} - \left(\frac{dP_1}{dt} \right)_{leak} \right] \quad (3.2)$$

in which permeability is in barrer (10^{-10} cm³ (STP).cm/sec/cm²/cmHg), V_d is the downstream volume, l is the membrane thickness, $\left(\frac{dP_1}{dt} \right)_{ss}$ is the steady state rate of pressure increase, $\left(\frac{dP_1}{dt} \right)_{leak}$ is the pressure leak rate, P_2 is the feed pressure, A is the membrane effective area, R is the universal gas constants and T is the operating temperature in kelvin.

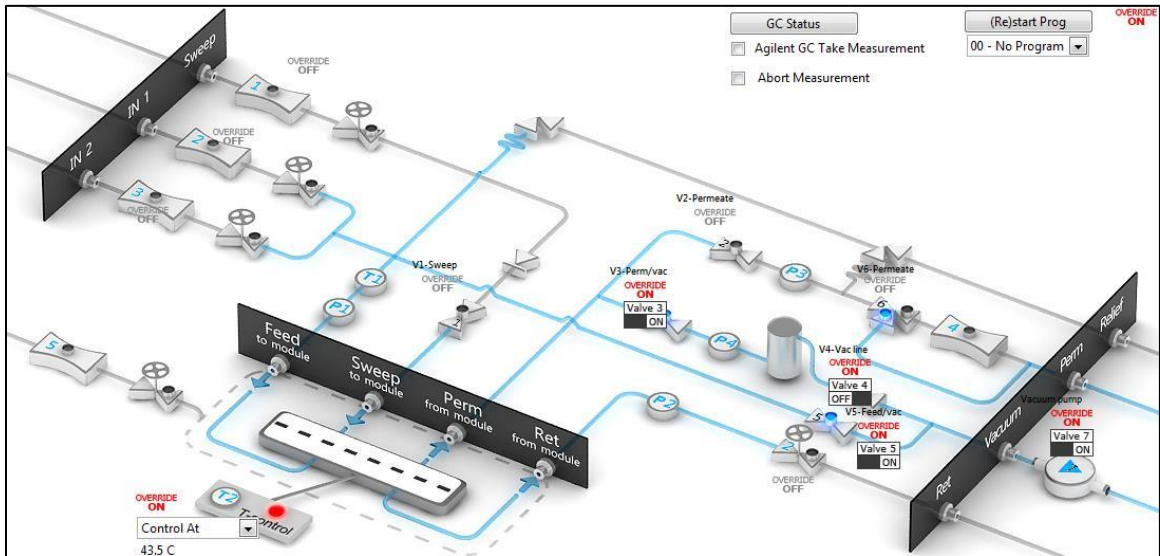


Figure 7: Schematic Diagram of Permeation Equipment

3.4.1 Temperature range

To study the effect of operating temperature, gas permeability measurements were conducted at different cell temperatures from 20 to 35°C at intervals of 5°C. The cell temperature was set by adjusting the oven temperature appropriately. During all measurements, feed temperature was recorded with an accuracy of $\pm 1^\circ\text{C}$.

The temperature range was carefully chosen based on thermodynamics of the gas. To keep the gas above the dew point line, phase diagram of some natural gas samples suggest the temperature to be above 50 F (10 °C, 283K) [47]. Furthermore, the triple point of CO₂ is at 5.1 atm and -56.6 °C while the critical point is at 73 atm and 31.1 °C. Tested operating temperature is in the range in which CO₂ is still in the gas state.

In addition, the temperature range of 20 – 35 °C is consistent the temperature range observed in the literature.

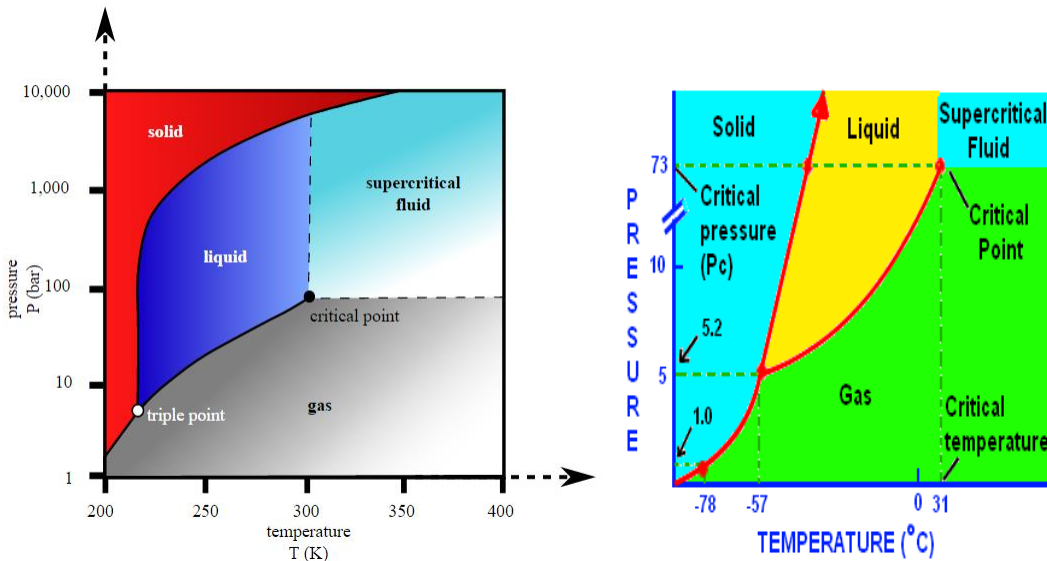


Figure 8: Phase diagram of CO₂

3.4.2 Pressure range

To study the effect of pressure, the feed pressure is varied from 1 barg to 5 barg and gas permeability measurements were conducted at these pressures. Variation of feed pressure was achieved by first setting the gas cylinder regulator to desired pressure and then opening the gas-in valve and setting it to control at maximum capacity. The main factors limiting the pressure range are thermodynamics and plasticization pressure. The pressure range 1 – 5 barg is far below the plasticization pressure of PSF which is the minimum pressure necessary to induce the permeability-increase. During plasticization, the polymer swells and therefore increases the permeability of CH₄ thereby causing decreased selectivity. CO₂ plasticization pressure of PSF membrane at 23 °C was found to be as high as 34 bar [48]. This pressure range is therefore a safe zone to avoid the interference of plasticization effect on membrane performance.

Practically, membrane systems are operated at very high feed pressures. For instance, the Kandawari plant, one of the largest membrane-based natural gas processing plants operates at 1305 psia.

CHAPTER 4

RESULTS AND DISCUSSIONS

This chapter details the results obtained from this research work. These include the results of characterizations of the fabricated membrane samples and the results of gas permeation. The effects of CDC loading, temperature and pressure on the performance of the mixed matrix membrane were also discussed.

4.1 Characterizations

4.1.1 Scanning Electron Microscopy

The SEM images showing the surface and cross section morphology of the pure and mixed matrix membranes are shown in Figure 9 and Figure 10. At the high SEM magnification of 20kx, the pure membrane exhibited no pores on the surface while its cross section image at 10kx magnification revealed a clean porous layer of sponge-like substructure underneath the top dense layer. This confirms the successful fabrication of asymmetric membranes comprising dense top layer and porous sub layer by the dry/wet phase inversion method, and therefore, gas permeation is expected to occur by solution-diffusion mechanism. A thin-selective layer was formed during the dry step of the phase inversion by evaporation of the volatile solvent (THF) to the surrounding while the

sponge-like substructure was formed as a result of the solvent exchange between the less volatile solvent (NMP) and water during the wet step [38].

As for the MMM, both the surface images and cross section images in Figure 9 and Figure 10 clearly indicate the presence CDC on the surface of the membranes and in the sub layer respectively. The tiny CDC particles are well dispersed at lower concentration and are therefore barely observed on the 0.1 and 0.5 wt % loaded membranes. At higher loadings, agglomeration begins to occur and increases with CDC loading - traces of agglomerations are observable at 1 wt% loading while they become much at the 2 wt% loading. Nanoparticles have tendency to form a bigger cluster as a result of the interaction between their surfaces, especially when a large number of the particles are incorporated [38]. The big agglomerations occurring at the 2 wt% loading may be attributed to the tendency of the nanoparticles to cluster together due to their high surface area.

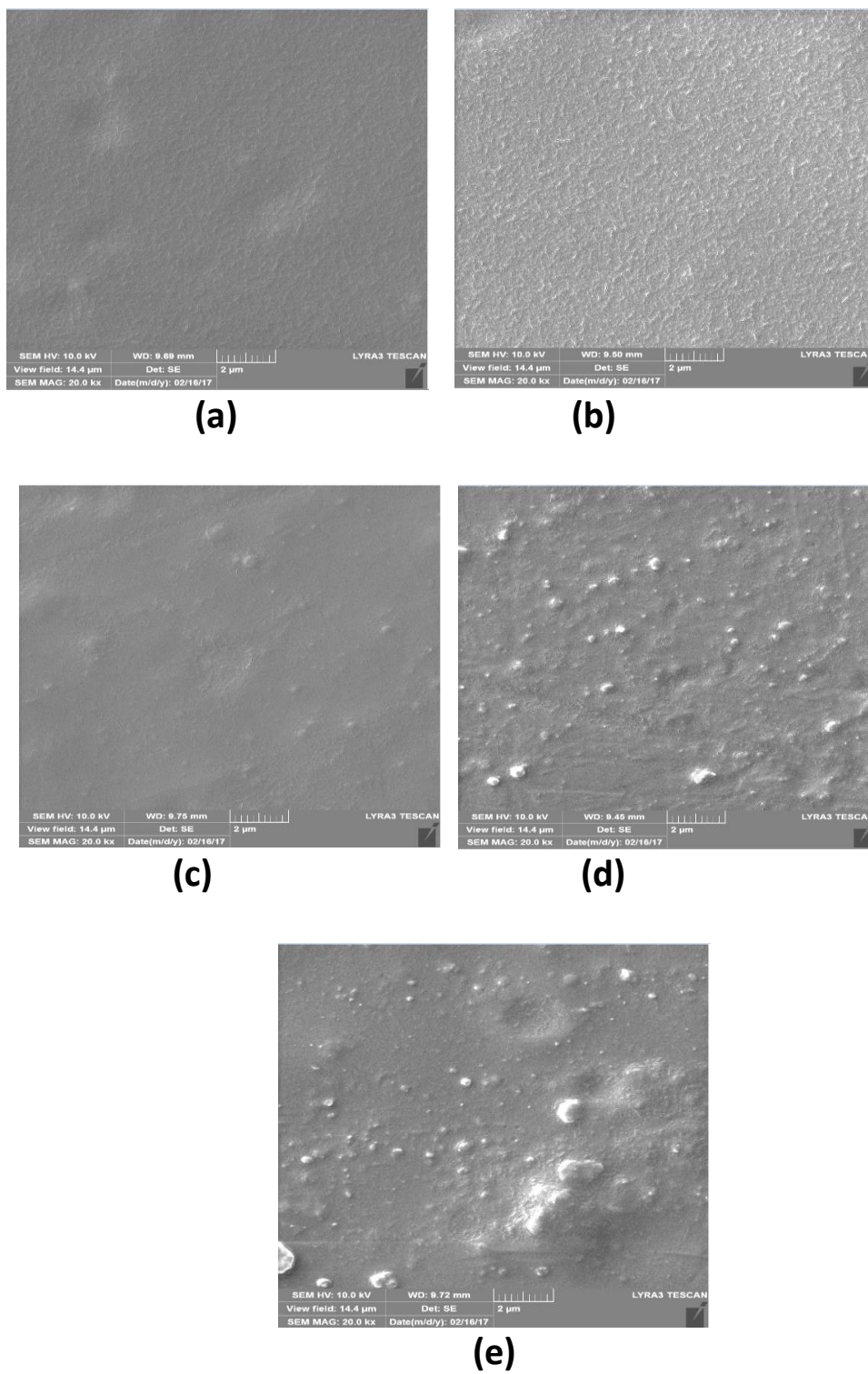
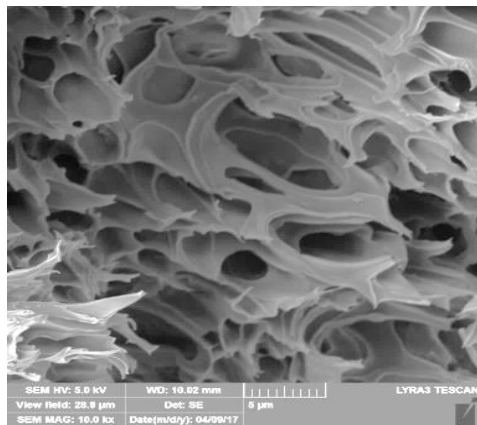
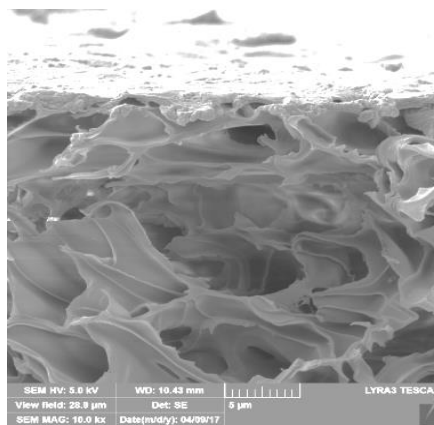


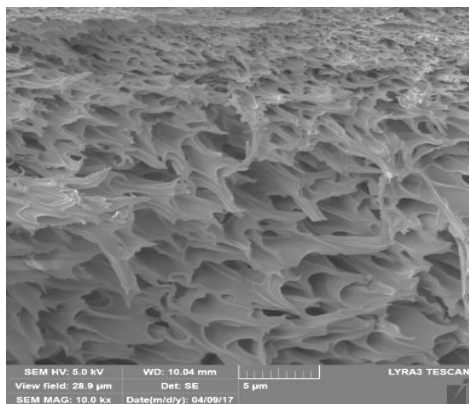
Figure 9: Surface SEM images of membrane samples at magnification of 20,000 – (a) Pure PSF membrane, (b) 0.1 wt% PSF/CDC membrane, (c) 0.5 wt% PSF/CDC membrane, (d) 1.0 wt% PSF/CDC membrane and (e) 2.0 wt% PSF/CDC membrane



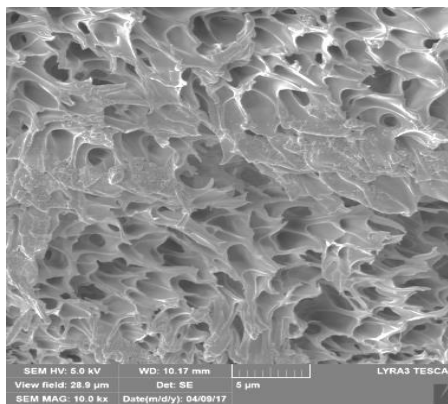
(a)



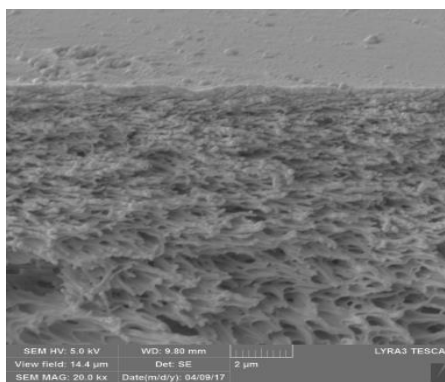
(b)



(c)



(d)



(e)

Figure 10: Cross section SEM images of membrane samples at magnification of 10,000– (a) Pure PSF membrane, (b) 0.1 wt% PSF/CDC membrane, (c) 0.5 wt% PSF/CDC membrane, (d) 1.0 wt% PSF/CDC membrane and (e) 2.0 wt% PSF/CDC membrane

4.1.2 X-ray diffraction

X-ray diffraction (XRD) patterns were reported for different CDC in the literatures. The XRD patterns of CaC_2 -CDC show the broad characteristic peaks at $2\theta = 26^\circ$, which correspond to diffraction from (002) planes of graphite [49]. The broad peaks suggest a highly disordered and amorphous structure of the CaC_2 -CDC [49]. Similarly, the two very broad peaks centered at the 2θ angles of $\sim 24^\circ$ and $\sim 44^\circ$ in the XRD pattern of TiC-CDC were attributed to diffuse scattering exhibited by the disordered carbon [50]. The two Bragg reflections centered at the 2θ angles of 24° and 44° were attributed to the (002) and (101) crystallographic planes of graphite [51]. The absence of sharp peaks corresponding to graphite in the XRD pattern of TiC-CDC further indicates the disordered nature of TiC-CDC and hence the amorphous nature of the carbon [18, 50].

The XRD pattern obtained for our synthesized TiC-CDC, shown in Figure 11, is very similar to CDC's XRD patterns [51] discussed above and therefore confirmed the synthesis of CDC from the TiC precursor. The displayed pattern in the figure reflects two broad peaks at 2θ approximately equal to 24 and 44. As explained above, the broad peaks correspond to diffractions from (002) and (101) crystallographic planes of graphite respectively and also indicate the disordered and amorphous nature of the synthesized CDC. However, some sharp peaks are observable at about 26 and 37 degree, even though they are of weak intensity. Furthermore, the XRD patterns are similar to those of other carbon materials. The two obtained peaks are also same for activated carbon [52, 53].

CDC demonstrates a wide variety of carbon phases. Amorphous and nanocrystalline graphitic carbons, in addition to nanotubes, fullerene-like structure, nanocrystalline diamond, and ordered graphite can be produced by selective etching of metal carbides

[14]. In fact, the structure of CDC is a heterogeneous mixture consisting of graphite, diamond, carbon onions, amorphous carbon, and carbon nanotube, since the synthesis temperature is below the graphitization temperature [54, 55].

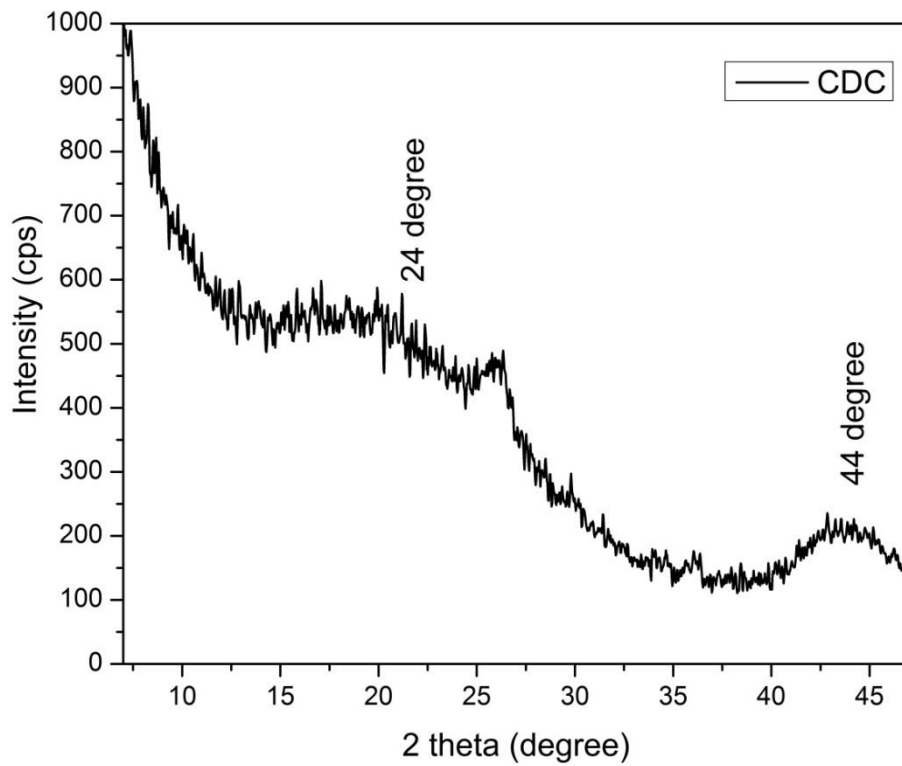


Figure 11: XRD pattern of CDC

The XRD patterns for the pure and mixed matrix membrane are shown in Figure 12. It is observed that the pure membrane has only one major broad peak at about 17 degree, which is characteristic of PSF. The broad peak depicts the amorphous nature of PSF. This

is consistent with XRD pattern of PSF in the literature. Furthermore, the XRD patterns of mixed membrane show the characteristic PSF broad peak in addition to two other peaks at 37 and 44 degree.

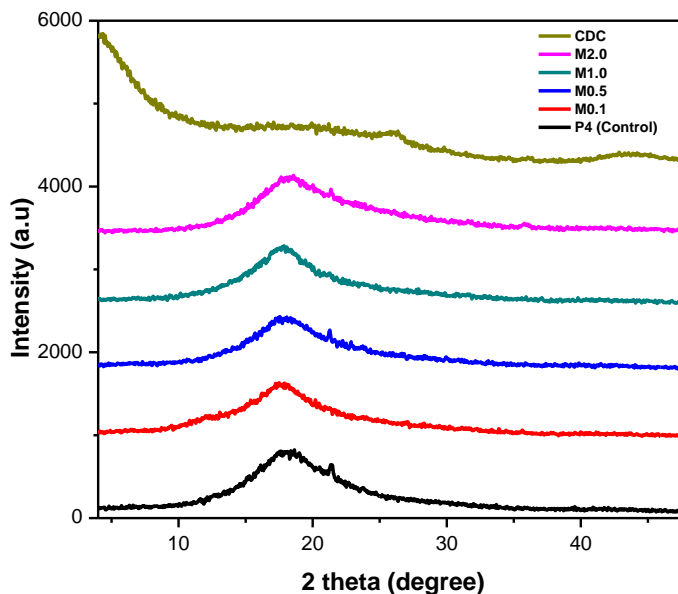


Figure 12: XRD patterns for pure membrane and mixed matrix membranes

4.1.3 Fourier Transform Infrared Spectroscopy (FTIR) results

FTIR spectra of CDC from different precursors are reported in literatures. For pure CDC derived from calcium carbide, characteristic peaks appeared at 3444 and 1096 cm^{-1} which are attributed to -OH and C-C-O stretching bands, respectively [49]. Several characteristic peaks detected for TiC-CDC produced at 600C at approximately 1392 , 1459 , 1646 , 2930 and 3490 cm^{-1} , corresponding to C-C , C-O , C=C , C-H and O-H stretching vibration bands, respectively, decrease sharply and even invisible for some of

them, for TiC-CDC produced at 1200 °C, which could be caused by the increased degree of graphitization [56].

The FTIR spectra obtained for the synthesized CDC using the KBr method, shown in Figure 13, is very similar to those obtained in the other works [49, 56]. Unlike organic carbons, pure CDC is considered to be real elemental carbon free of surface compounds, such as hydrogen and oxygen [14, 57]. This is because it is produced from the selective etching of metal from metal carbide as illustrated schematically in Figure 14a. However, the obtained spectrum shows more than one peaks between the ranges of 700 – 4000 cm^{-1} wavenumber. These multiple peaks are highlighted in Table 9. The peaks can be attributed to the nature and surface chemistry of CDC.

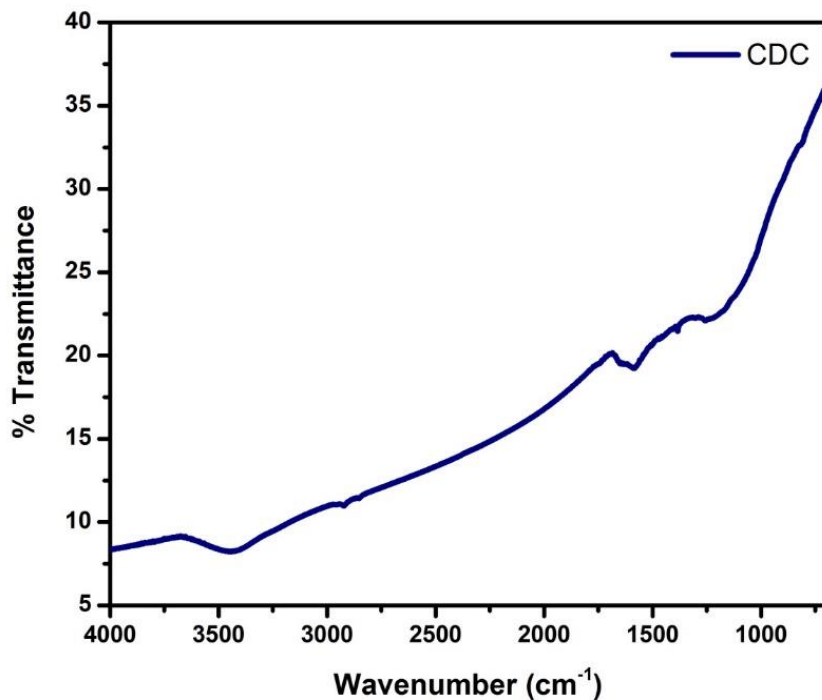


Figure 13: FTIR Spectra of CDC

The amorphous structure type of CDC can be responsible for some of the peaks found in the CDC spectra. Diamond comprises a fully tetrahedral sp^3 -hybridised C-C bonding configuration with 4 sigma bonds while graphite is a fully trigonal sp^2 network that forms planar six-fold rings of single and double bonds, with weak van der Waals bonding between planes. However, amorphous carbon films can form with a mixture of any of these bonds including sp^1 with other carbon atoms or impurities (dopants). In other words, the microstructure of amorphous carbon allows the coexistence of sp^1 , sp^2 and sp^3 bonds in both the carbon systems and with other impurities existing in the microstructure. This gives rise to some of the advantageous and variable material properties of amorphous carbon [58].

Surface chemistry of CDC further justifies the presence of other several peaks on the FTIR spectra. The surface chemistry of carbon is generally related to the presence of heteroatoms such as oxygen, hydrogen, phosphorus, sulfur and nitrogen), which are bonded at the edges of the graphite-like layers and form organic functional groups [59]. Amorphous carbons have tendency to chemisorb oxygen than ordered carbon [60] and CDC is also said to be very hygroscopic after synthesis and can absorb up to 35% of their weight in water in low humidity environments [54, 55]. Therefore, the exposure of CDC, especially those synthesized at low temperature, to ambient air can give rise to the formation of oxygen surface moieties and this can be caused as a result of chemical interaction with water and/or oxygen [61]. During exposure to air, oxidation and/or gasification of the carbon occur [62], and consequently, acid anhydride and/or lactone complexes are formed on carbon surface [62]. Some of these formed species may further be hydrolyzed by the moisture in the air to form carboxylic acid groups [62]. Overall, the surface functionalities of carbon as a result of exposure to ambient air may include that of ketones, carboxyl, carboxyl anhydride, and lactone [61, 63-65]. Specifically for CDC, it was established that the surface of CDC possess oxygen functional groups such as carboxylic acids, carboxylic anhydrides, phenols and lactones [59]. In fact, the surface chemistry of CDC can be described by the model shown in the Figure 14b [60, 64].

Table 9: Peak Identification of CDC FTIR

Major Peaks	Identification in the range	Functionality
3446	-OH [56]	hydroxyl
2922	C-H stretching [66]	Aliphatics
2854	Methylene symmetric C-H bending [56, 66]	Aliphatics
1651	C=O, C=C (olefin) [58]	Carbonyl/ketone
1585	C=C (aromatic) [58]	Aromatics
1384	C-C [56], sp ³ Methyl symmetrical C-H Bending [66]	Aliphatics

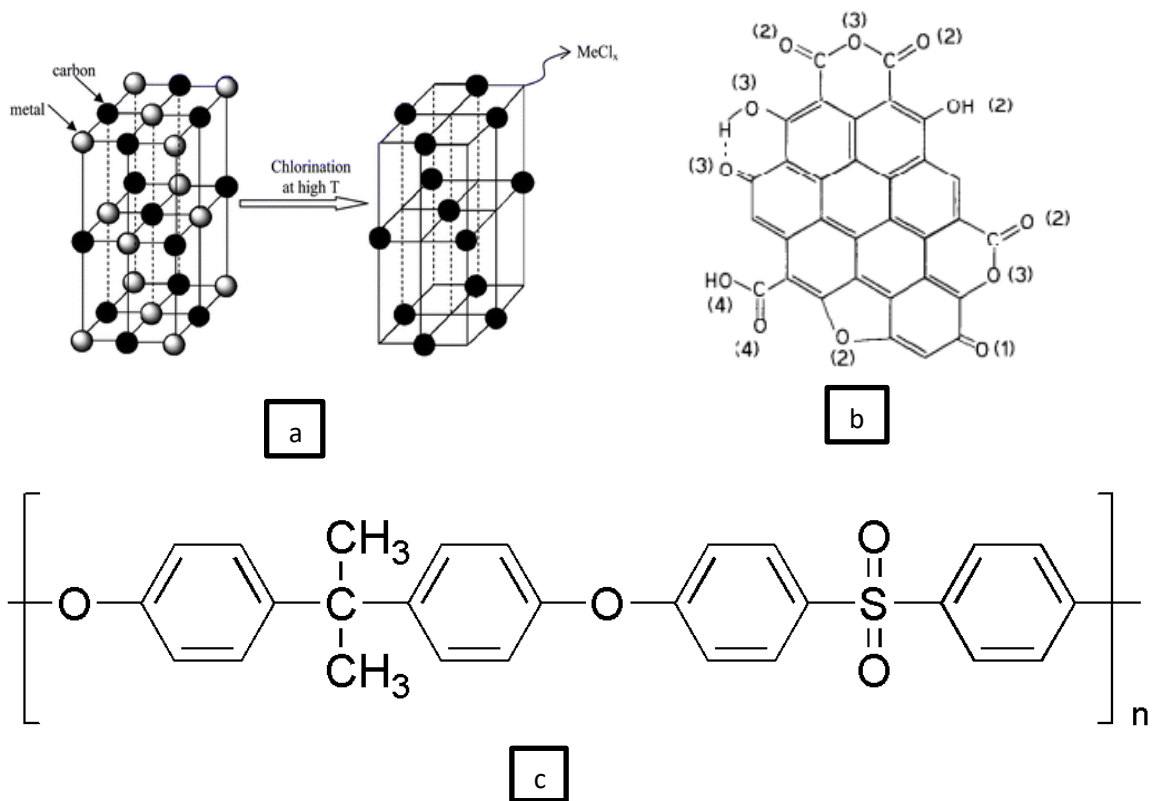


Figure 14: (a) Schematic illustration of the selective chlorination of a metal carbide lattice with a fcc structure [67], (b) CDC model showing surface chemistry, (c) chemical structure of PSF.

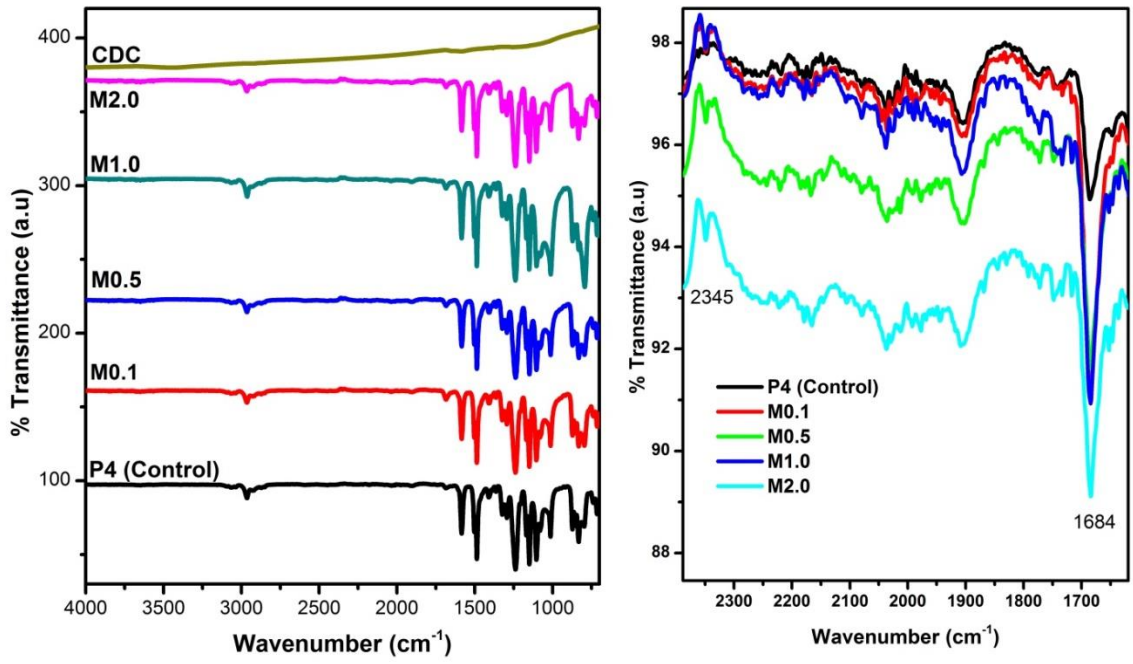


Figure 15: FTIR spectra of pure membrane and MMM

Table 10: Major Peaks of PSF FTIR spectra

S/N	Major Peaks	Identification in the range
1	2964	CH ₃ [68]
2	1584	C=C of aromatic [68, 69]
3	1487	asymmetric deformation due to vibration of OH [68], aromatic C=C ([69]
4	1410	Asymmetric C-H bending deformation of methyl group [69]
5	1363	Symmetric deformation due to vibration of OH [68], symmetric C-H bending deformation of methyl group [69]
6	1324	O=S=O [68]
7	1294	O=S=O [68]
8	1239	Asymmetric C-O-C stretching of aryl ether group [69]
9	1149	O=S=O [70]
10	1104	Aromatic ring vibration [69]
11	1080	Aromatic ring vibration [69]

The FTIR spectra of pure PSF and mixed matrix membranes are shown in Figure 15. The pure PSF FTIR spectra is similar to reported spectra in the literature [71]. The FTIR spectrum of pure PSF membrane shows characteristic infrared bands at around 1149 cm^{-1} and 1168 cm^{-1} for the SO_2 symmetric stretch, 1243 cm^{-1} for the Aryl-O-aryl C-O stretch, 1325 cm^{-1} for SO_2 asymmetric stretch, 1380 cm^{-1} (asymmetric- CH_3), and 1583 cm^{-1} for (C=C) stretching vibrations of aromatic rings [34, 72, 73]. In addition, the peak at ~ 2873 , 2966 and 3094 cm^{-1} show characteristic infrared bands of CH_3 -symmetric aliphatic stretch, CH_3 -asymmetric aliphatic stretch and C-H aromatic stretch respectively [73]. The FTIR spectra of PSF/CDC MMM are similar to that of pure PSF membrane, but the difference is best portrayed after further analysis of results as shown in Figure 15b. One of the major differences is the C=O bond in carboxyl groups around 1680 cm^{-1} occurring in the MMMs, which is attributed to CDC. The occurrence of peak at 1680 cm^{-1} can be explained in that the CDC's presence in the mixed matrix membrane could affect the concentration of carboxylic groups on the surface of MMMs. Furthermore, the intensity of these peaks enhances with increasing CDC loading in the PSF polymer matrix [34]. For higher CDC incorporation, the CDC aggregate causes much stronger peak than those with lower CDC concentrations. The presence of this carboxyl in mixed matrix membrane can influence the gas permeability [34]

4.1.4 Thermogravimetric analysis TGA

Thermo gravimetric studies were performed in order to investigate the thermal stability of CDC and the effect of incorporation of the CDC particles on the thermal stability of the mixed matrix membrane containing them.

Figure 16 shows the TGA curves of CDC, pure PSF membrane and all the mixed matrix membrane samples. CDC exhibits steady weight loss from 30 °C to less than 100 °C, after which the weight loss is almost negligible. For pure PSF and the mixed matrix membranes, the first weight loss was exhibited at the temperature of about 110 °C and this can be attributed to the loss of moisture trapped in the membrane during the wet phase inversion. The second weight loss occurring at around temperature of 500 °C is attributed to the degradation of the actual membrane material. No significant difference between thermal stability of pure membrane and MMMs is observed, except for the obvious variation in samples' residuals.

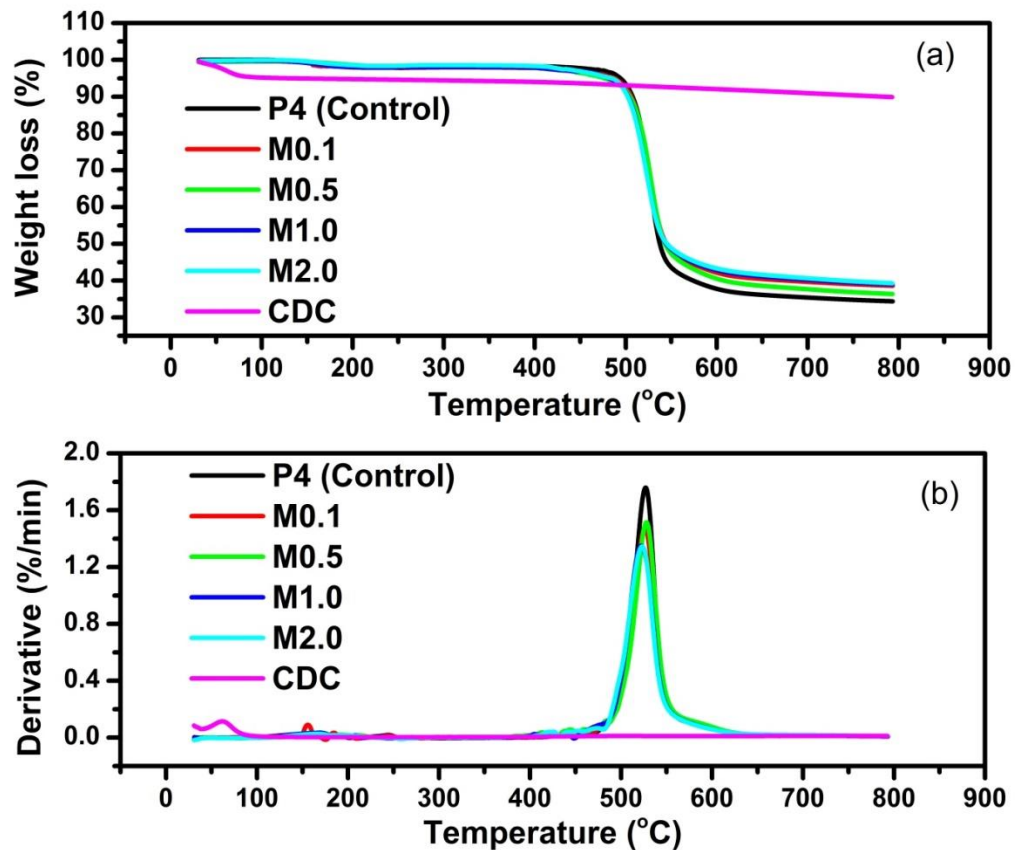


Figure 16: TGA curves of pure and mixed matrix membrane

However for detailed comparison, Table 11 shows the parameters obtained by further analysis of the TGA curves of all the samples. These parameters give more insight about the effect of filling PSF matrix with CDC on the thermal stability of the membranes.

Table 11: TGA data for CDC and membrane samples

Sample	Onset temp (°C)	T_{5%} (°C)	T_{10%} (°C)	T_{50%} (°C)	Total residue (wt%)
P4 (Control)	507.84	494.18	507.52	537.49	34.37
M0.1	505.66	487.61	506.01	544.90	38.60
M0.5	506.07	476.34	504.72	543.17	36.34
M1.0	500.09	481.53	502.82	544.53	39.02
M2.0	499.42	484.45	502.18	545.42	39.27
CDC	*ND	128.12	789.00	*ND	89.88

*ND = Not detectable

The non-detectable onset temperature and T_{50%} values in addition to the high T_{10%} and total residue values of CDC within the tested temperature range indicate that CDC exhibits extremely high thermal stability. However, due to the hygroscopic nature of CDC [54, 55], the high amount of water absorbed is lost at the low temperature range and this is responsible for the low value of T_{5%} and the maximum weight loss occurring at low temperature (65 °C).

Furthermore, for the mixed matrix membranes, the total residue and T_{50%} values are generally increased with increasing CDC loading. This clearly indicates the thermal stability reinforcement of the membrane by the CDC. Meanwhile, decreasing values of onset temperature, T_{5%} and T_{10%} are observed at increasing CDC loading and this could

be attributed to the low $T_{5\%}$ and the low temperature - maximum weight loss of the incorporated CDC.

4.2 Gas permeation

4.2.1 Effect of polymer concentration

Optimization of formula for the control PSF membrane was performed using the dry/wet phase inversion method by adjusting PSF polymer concentration. The formula contains a mixture of solvents and non-solvents together with a variable concentration of PSF. A mixture of solvents is reported to be good for tuning the asymmetric membrane characteristics formed by the dry/wet phase inversion [33]. In this part of the research, a combination of NMP and THF were used as the mixture of solvents in a fixed ratio of 3:1 while ethanol (as a non-solvent) was used at a constant concentration of 10 wt%. Excess of the more volatile solvent in the composition may result in the formation of porous top layer during the drying step and hence NMP was used as the excess solvent. NMP has low volatility, high affinity for water and high interaction with PSF polymer while THF has exactly the opposite of these features. The high volatility of THF and its low interaction with PSF are important for creating thin-dense top-layer in the dry step of the membrane fabrication while the high affinity of NMP for water is important for the formation of the porous under-layer in the wet step. In addition, ethanol (non-solvent) was added to increase the turbidity and favorably alter the phase behavior during membrane formation.

The effect of PSF concentration was studied based on its effect on membrane permeance and selectivity. Five membranes with different PSF concentrations varying from 15 – 35 wt% were prepared and tested for CO₂ and CH₄ gas permeation. As shown in Figure 17, the membrane permeance of CO₂ and CH₄ decreases as the PSF concentration increases from 15 wt% to 30 wt% with a corresponding increase in selectivity, beyond which the permeance begins to increase with a corresponding decrease in selectivity.

This trend is consistent with similar work in the literature [33, 74]. Most likely, a dilute PSF solution results in a thin skin layer which is susceptible to defects, thereby leading to a porous membrane with high permeance and low gas selectivity. However, increasing the polymer concentration generates a more viscous polymer solution which produces a membrane with denser and thicker skin layer, thereby promoting low gas permeance and high gas selectivity. Therefore, there exists a critical PSF polymer concentration which gives rise to a membrane with optimum performance in terms of permeance and selectivity. Based on the data presented in Figure 17, the optimum PSF concentration in the formulation is 30 wt% and this produces a membrane with a CO₂ permeance and CO₂/CH₄ selectivity of 2.5 GPU and 12.1; respectively. This optimized formulation was consequently used for effect of loading study.

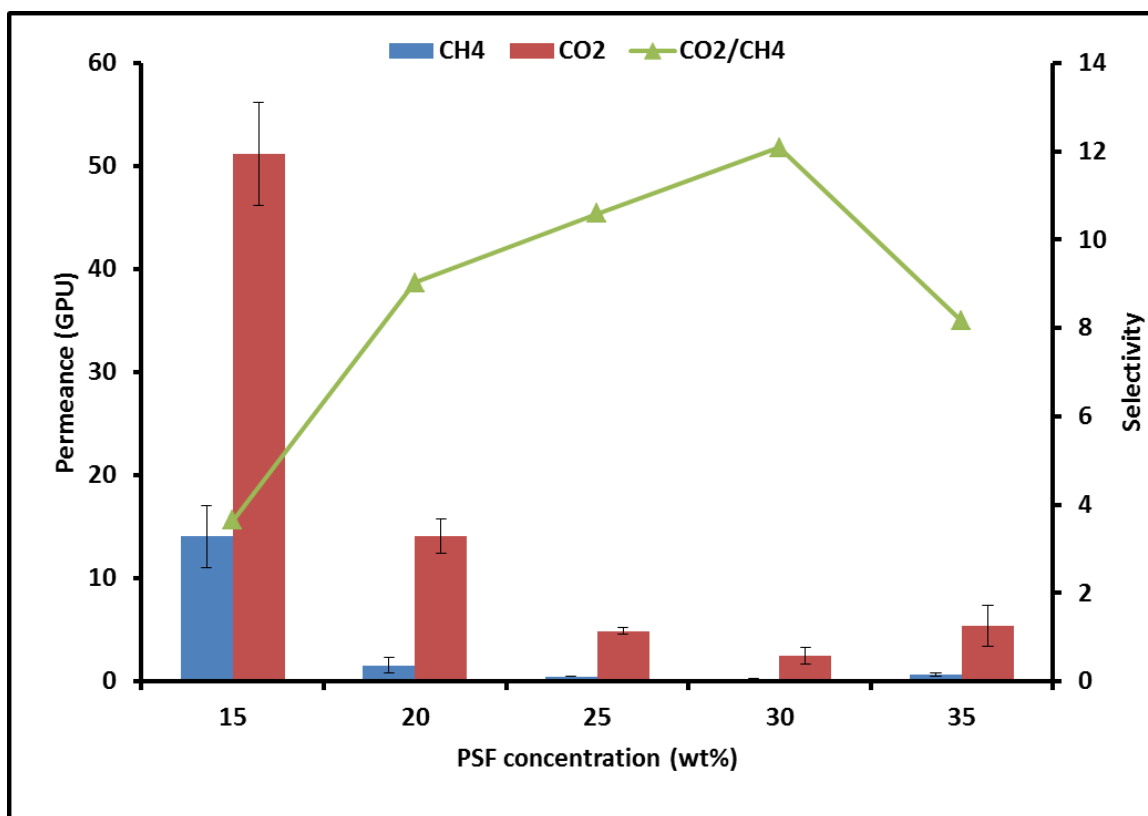


Figure 17: Effect of PSF concentration on gas permeance and selectivity

4.2.2 Effect of loading

The effect of CDC loading on the gas permeation properties of PSF-based mixed matrix membrane was investigated with a loading range from 0.1 to 2 wt%. This range was selected because some carbon materials are generally required in low quantity for developing mixed matrix membrane. Several mixed matrix membrane containing carbon materials such as CNF [34], functionalized multi-walled carbon nanotubes membrane [43] and a novel carbon nanoparticle [28] were investigated at loadings not more than 4% with agglomeration usually occurring at 1 wt% loading.

The permeance and selectivity of the control and mixed matrix membrane were tested at 20 °C and 5 barg as shown in Figure 18. Up to 0.5 wt% loading, there is increase in membrane permeance of both CO₂ and CH₄ which can be explained by increased solubility and/or diffusivity. Diffusivity will always be enhanced either as a result of the gas transport channels provided by the nanoporous CDC in the matrix according to Maxwell's and Nelson's Models [38, 75] or as a result of disruption of polymer chain packing which induces excess free volume for permeation boosting [75]. While increased diffusivity due to the incorporation of CDC contributes to permeance enhancements of both CO₂ and CH₄ gases, permeance of CO₂ is additionally enhanced by solubility factor due to increased polarity as confirmed by the FTIR results. Consequently, the increase in permeance of CO₂ (120% at 0.5 wt% loading) greatly surpasses that of CH₄ (70.3% at 0.5 wt% loading) and hence increased CO₂/CH₄ selectivity with loading is obtained.

Above 0.5 wt% loading, there is decreased permeance of the gases through the mixed matrix membrane. It is possible that both the diffusivity and solubility have been jeopardized at these higher loadings. As confirmed from the SEM analysis, agglomeration began from 1 wt% and became worse at 2 wt%. Most probably, this is a case of agglomeration without interfacial defect and the agglomeration is solely causing partial or full blockage of the diffusion path created by the nanoporous CDC in the polymer matrix. In other words, polymer rigidification occurs as a result of the polymer/filler contact leading to lower gas diffusion [76]. In addition, the agglomeration reduces uniform dispersion of the fillers in the matrix and causes formation of clusters thereby increasing the potential of reducing the solubility effectiveness of the CDC

particles in the PSF matrix. The maximum CO_2/CH_4 selectivity of 27 corresponding to 123% selectivity increase over that of the control membrane occurs at 1 wt% loading.

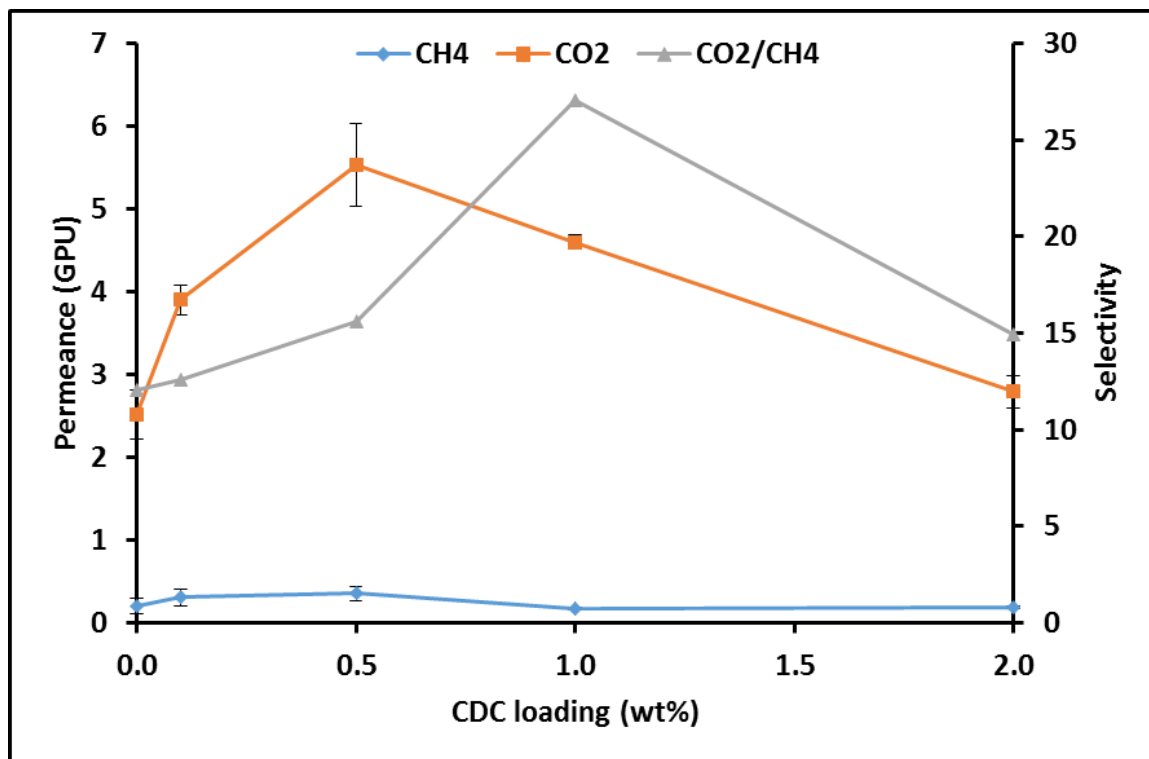


Figure 18: Effect of CDC loading on permeance and selectivity

The increased solubility and hence solubility selectivity of the MMMs attributed to the effect of CDC can be related to the surface chemistry of the CDC. FTIR data presented earlier revealed the presence of oxygen surface complexes on the CDC surface and consequently in the mixed matrix membrane. These oxygen complexes influence the carbon behavior to as much great extent as relevant in the mixed matrix membrane. It has a significant influence on the performance of membranes because they promote the polarity. Hence, CDC with a polar surface can enhance the performance of gas

membranes separating a mixture of polar and non-polar components. The carbonyl group, confirmed by FTIR, has interaction with polar gas -such as CO₂- than non-polar gas – such as CH₄,- thereby enhancing the polar gas solubility and selectivity. This is consistent with the enhancement of CO₂/CH₄ selectivity by polarity due to the presence of carbonyl group on the surface of CNF [34] and modified CNT [77].

4.2.3 Effect of temperature

Since the 1 wt% CDC loading membrane showed the highest selectivity, it was chosen for further study to investigate the effect of operating temperature on the permeation properties of the membrane as shown in Figure 19. Feed gas was at 5 barg pressure while the temperature was in the range of 20 to 35 °C. For both CO₂ and CH₄ gases, permeance increased with the operating temperature. Generally, for a glassy polymer such as PSF, the diffusivity increases with temperature due to increased flexibility of the polymer chains [78, 79]. However, the degree of temperature effect differs for the two gases. The effect of temperature is more pronounced on CH₄ permeation than CO₂ permeation and this is responsible for the decreasing CO₂/CH₄ selectivity with increasing temperature as illustrated in Figure 19. Contrary to the effect of temperature on permeance, temperature has an opposite effect on selectivity. Based on the data in Figure 19, low temperature favors good separation performance of the membrane.

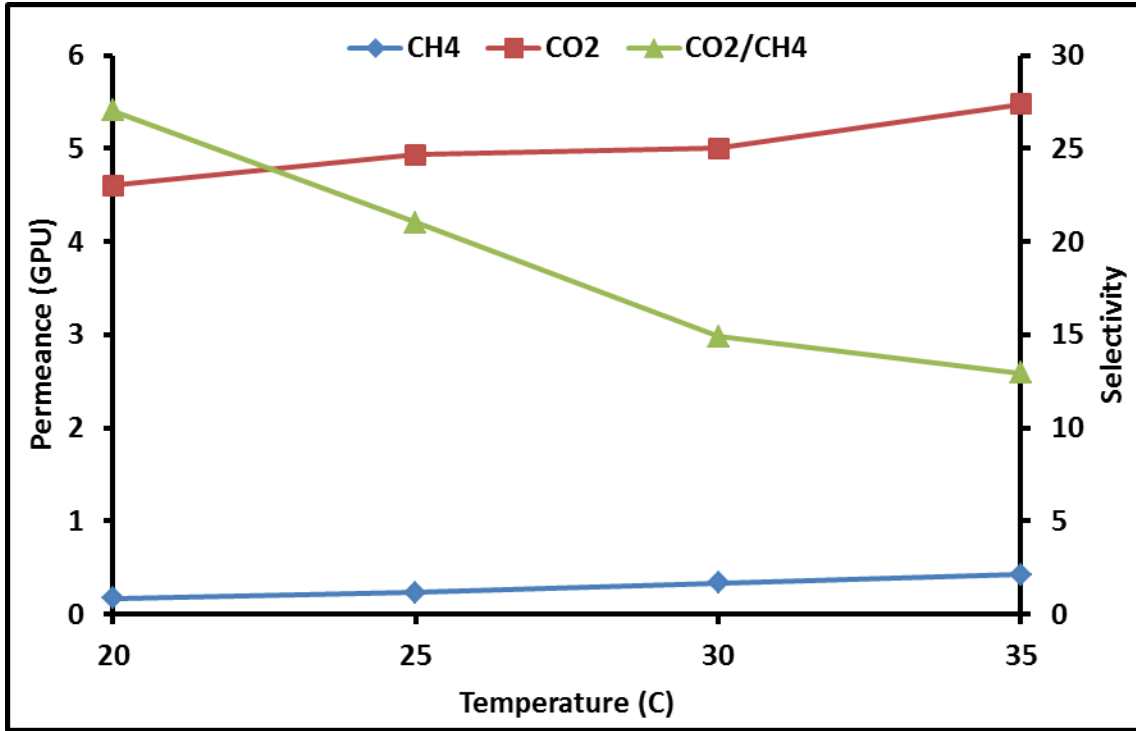


Figure 19: Effect of temperature on gas permeance and selectivity of 1 wt% MMM

The Arrhenius equation relating gas permeability to operating temperature can be used to further describe the temperature dependence of gas permeability as expressed by the following equation [80]:

$$P = P_0 \exp\left(-\frac{E_p}{RT}\right) \quad (4.1)$$

where P is the permeability of the gas, P_0 the pre-exponential factor, E_p is the activation energy of permeation, R the gas constant and T the absolute temperature. E_p directly and quantitatively indicates the extent of dependence of gas permeability on temperature.

Equation 2 can be linearized to the form of Equation 3:

$$\ln(P) = \ln(P_0) - \frac{E_P}{R} \frac{1}{T} \quad (4.2)$$

The permeance data of CH₄ and CO₂ were fitted to the linearized form of Arrhenius equation and showed an excellent agreement with the correlation coefficients of 0.995 and 0.932; respectively. Consequently, E_P values of 46.4 and 8.1 kJ/mol were calculated for CH₄ and CO₂; respectively. Both values are positive, implying that the temperature has a positive effect on permeance of the gases [78]. Furthermore, the values also suggest that the effect of temperature is more pronounced on the permeation of CH₄ than that of CO₂ due to higher activation energy of permeation of CH₄.

4.2.4 Effect of pressure

The effect of feed pressure on the membrane permeance and selectivity was evaluated for the 1 wt% membrane at temperature of 20 °C. Gas permeation experiments were carried out at feed pressures of 1 – 5 barg for both CO₂ and CH₄ gases and the results are shown in Figure 20. Generally, there is decreased permeance of both CO₂ and CH₄ gases as the pressure is increased. This is because the adsorption capacity of the mixed matrix membrane becomes saturated at elevated pressure [78]. In addition, dual-mode sorption model explaining the pressure dependence of gas permeability describes gas transport in glassy polymers and indicates that gas permeability reduces with increasing pressure [35, 46]. However, it is shown that the extent of pressure dependence of CO₂ permeance differs from that of CH₄, thus a change in CO₂/CH₄ selectivity with pressure is obtained. Overall, increasing feed pressure favors increased CO₂/CH₄ selectivity.

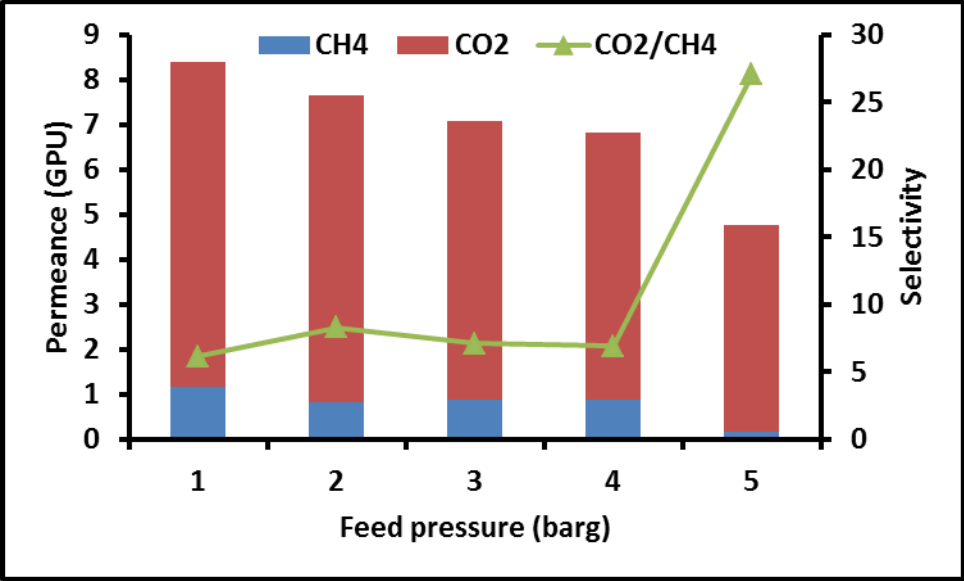


Figure 20: Effect of feed pressure on performance of 1 wt% mixed matrix membrane

CHAPTER 5

CONCLUSIONS AND RECOMMENDATIONS

5.1 Conclusions

This study concludes with the following:

1. An ultrathin and defect-free asymmetric pure polysulfone membrane suitable for CO₂/CH₄ separation was successfully developed using the dry/wet phase inversion technique via optimization of the formulation.
2. Carbide derived carbon was successfully incorporated in PSF matrix for development of mixed matrix membrane for CO₂/CH₄ separation.
3. Incorporation of CDC caused unchanged amorphous nature of the membrane, reinforced thermal stability, uniform dispersion up to 0.5 wt% loading and imparted polarity due to the favorable surface chemistry of CDC.
4. MMMs have better separation performance than the pure PSF membrane; CO₂ permeance increased by 120 % at 0.5 wt% loading and best CO₂/CH₄ selectivity of 27 at 1% loading was achieved.
5. The improvement in separation performance was due to enhanced solubility based on polarity and enhanced diffusivity as a result of creation of diffusivity channel by the nanoporous CDC.

6. Low temperature and higher feed pressure favour better performance of the 1wt% mixed matrix membrane

5.2 Recommendations

The following points are hereby recommended for future studies.

1. High pressure studies of the PSF/CDC mixed matrix membrane should be done to confirm the prediction in this study
2. CDC can be incorporated in other commercial polymer matrix such as polyimide
3. CDC can be oxidized and then investigated as fillers in mixed matrix membrane
4. Due to the high surface area of CDC, it can be functionalized and then investigated as fillers in mixed matrix membrane.

References

- [1] R. W. Baker and K. Lokhandwala, "Natural Gas Processing with Membranes: An Overview," *Industrial & Engineering Chemistry Research*, vol. 47, pp. 2109-2121, 2008/04/02 2008.
- [2] A. Demirbas, "The importance of natural gas as a world fuel," *Energy Sources, Part B*, vol. 1, pp. 413-420, 2006.
- [3] http://www.lukoil.com/materials/doc/documents/global_trends_to_2025.pdf.
- [4] <http://www.shearman.com/~media/Files/NewsInsights/Publications/2016/09/Saudi-Arabia-Publications/Oil--Gas-in-the-Kingdom-of-Saudi-Arabia--An-Overview.pdf>.
- [5] <https://www.worldenergy.org/data/resources/country/saudi-arabia/gas/>.
- [6] <http://www.saudiaramco.com/en/home/our-business/sustaining-excellence/gas-development.html>.
- [7] <http://www.jeg.org.sa/data/modules/contents/uploads/infopdf/2799.pdf>.
- [8] http://www.rigzone.com/news/oil_gas/a/138519/Saudi_Aramco_Discovered_Eight_New_Oil_and_Gas_Fields_in_2014.
- [9] <http://www.naturalgasasia.com/saudi-aramaco-discovered-eight-new-oil-gas-fields-in-2014-15527>.
- [10] <http://www.naturalgasasia.com/category/news-by-country/saudi-arabia>.

- [11] T. Cnop, D. Dortmund, and M. Schott, "Continued development of gas separation membrane for highly sour service," *UOP LLC, Illinois, USA*, 2007.
- [12] D. R. Paul and Y. P. Yampol'skii, *Polymeric gas separation membranes*: CRC press, 1993.
- [13] Y. Manawi, V. Kochkodan, M. A. Hussein, M. A. Khaleel, M. Khraisheh, and N. Hilal, "Can carbon-based nanomaterials revolutionize membrane fabrication for water treatment and desalination?," *Desalination*, vol. 391, pp. 69-88, 8/1/ 2016.
- [14] Y. Gogotsi and V. Presser, *Carbon nanomaterials*: CRC Press, 2013.
- [15] V. Presser, M. Heon, and Y. Gogotsi, "Carbide-Derived Carbons—From Porous Networks to Nanotubes and Graphene," *Advanced Functional Materials*, vol. 21, pp. 810-833, 2011.
- [16] R. K. Dash, A. Nikitin, and Y. Gogotsi, "Microporous carbon derived from boron carbide," *Microporous and Mesoporous Materials*, vol. 72, pp. 203-208, 7/8/ 2004.
- [17] R. K. Dash, G. Yushin, and Y. Gogotsi, "Synthesis, structure and porosity analysis of microporous and mesoporous carbon derived from zirconium carbide," *Microporous and Mesoporous Materials*, vol. 86, pp. 50-57, 11/28/ 2005.
- [18] R. Dash, J. Chmiola, G. Yushin, Y. Gogotsi, G. Laudisio, J. Singer, *et al.*, "Titanium carbide derived nanoporous carbon for energy-related applications," *Carbon*, vol. 44, pp. 2489-2497, 10// 2006.
- [19] J. Zheng, T. C. Ekstrom, S. K. Gordeev, and M. Jacob, "Carbon with an onion-like structure obtained by chlorinating titanium carbide," *Journal of Materials Chemistry*, vol. 10, pp. 1039-1041, 2000.

- [20] S. Welz, M. J. McNallan, and Y. Gogotsi, "Carbon structures in silicon carbide derived carbon," *Journal of Materials Processing Technology*, vol. 179, pp. 11-22, 10/20/ 2006.
- [21] Y. Gogotsi, A. Nikitin, H. Ye, W. Zhou, J. E. Fischer, B. Yi, *et al.*, "Nanoporous carbide-derived carbon with tunable pore size," *Nat Mater*, vol. 2, pp. 591-594, 09//print 2003.
- [22] J. Torop, T. Sugino, K. Asaka, A. Jänes, E. Lust, and A. Aabloo, "Nanoporous carbide-derived carbon based actuators modified with gold foil: Prospect for fast response and low voltage applications," *Sensors and Actuators B: Chemical*, vol. 161, pp. 629-634, 1/3/ 2012.
- [23] T. Thomborg, A. Jänes, and E. Lust, "Energy and power performance of vanadium carbide derived carbon electrode materials for supercapacitors," *Journal of Electroanalytical Chemistry*, vol. 630, pp. 55-62, 5/15/ 2009.
- [24] S.-H. Yeon, S. Osswald, Y. Gogotsi, J. P. Singer, J. M. Simmons, J. E. Fischer, *et al.*, "Enhanced methane storage of chemically and physically activated carbide-derived carbon," *Journal of Power Sources*, vol. 191, pp. 560-567, 6/15/ 2009.
- [25] Y. Gogotsi, R. K. Dash, G. Yushin, T. Yildirim, G. Laudisio, and J. E. Fischer, "Tailoring of nanoscale porosity in carbide-derived carbons for hydrogen storage," *Journal of the American Chemical Society*, vol. 127, pp. 16006-16007, 2005.
- [26] H. S. Kim, J. P. Singer, Y. Gogotsi, and J. E. Fischer, "Molybdenum carbide-derived carbon for hydrogen storage," *Microporous and Mesoporous Materials*, vol. 120, pp. 267-271, 4/15/ 2009.

- [27] S. Porada, L. Borchardt, M. Oschatz, M. Bryjak, J. Atchison, K. Keesman, *et al.*, "Direct prediction of the desalination performance of porous carbon electrodes for capacitive deionization," *Energy & Environmental Science*, vol. 6, pp. 3700-3712, 2013.
- [28] R. Mukherjee and S. De, "Novel carbon-nanoparticle polysulfone hollow fiber mixed matrix ultrafiltration membrane: Adsorptive removal of benzene, phenol and toluene from aqueous solution," *Separation and Purification Technology*, vol. 157, pp. 229-240, 1/8/ 2016.
- [29] A. Shahtalebi, M. Mar, K. Guérin, and S. K. Bhatia, "Effect of fluorine doping on structure and CO₂ adsorption in silicon carbide-derived carbon," *Carbon*, vol. 96, pp. 565-577, 1// 2016.
- [30] S.-M. Hong, S. W. Choi, S. H. Kim, and K. B. Lee, "Porous carbon based on polyvinylidene fluoride: Enhancement of CO₂ adsorption by physical activation," *Carbon*, vol. 99, pp. 354-360, 4// 2016.
- [31] E. N. Hoffman, G. Yushin, B. G. Wendler, M. W. Barsoum, and Y. Gogotsi, "Carbide-derived carbon membrane," *Materials Chemistry and Physics*, vol. 112, pp. 587-591, 12/1/ 2008.
- [32] M. Pakizeh, S. Mansoori, M. Pourafshari Chenar, and M. Namvar-Mahboub, "Modification of PSf membrane nanostructure using different fabrication parameters and investigation of the CO₂ separation properties of PDMS-coated PSf composite membranes," *Brazilian Journal of Chemical Engineering*, vol. 30, pp. 345-354, 2013.

- [33] S. C. Pesek and W. J. Koros, "Aqueous quenched asymmetric polysulfone membranes prepared by dry/wet phase separation," *Journal of membrane science*, vol. 81, pp. 71-88, 1993.
- [34] A. Dehghani Kiadehi, A. Rahimpour, M. Jahanshahi, and A. A. Ghoreyshi, "Novel carbon nano-fibers (CNF)/polysulfone (PSf) mixed matrix membranes for gas separation," *Journal of Industrial and Engineering Chemistry*, vol. 22, pp. 199-207, 2/25/ 2015.
- [35] J. Ahn, W.-J. Chung, I. Pinnau, and M. D. Guiver, "Polysulfone/silica nanoparticle mixed-matrix membranes for gas separation," *Journal of Membrane Science*, vol. 314, pp. 123-133, 4/30/ 2008.
- [36] B. Zornoza, A. Martinez-Joaristi, P. Serra-Crespo, C. Tellez, J. Coronas, J. Gascon, *et al.*, "Functionalized flexible MOFs as fillers in mixed matrix membranes for highly selective separation of CO₂ from CH₄ at elevated pressures," *Chemical Communications*, vol. 47, pp. 9522-9524, 2011.
- [37] A. U. H. Khan, "Water desalination using carbide derived carbon (CDC)/ Mixed Matrix membrane," Masters of Science, Chemical Engineering, King Fahd University of Petroleum and Minerals, 2016.
- [38] N. A. H. M. Nordin, A. F. Ismail, A. Mustafa, R. S. Murali, and T. Matsuura, "Utilizing low ZIF-8 loading for an asymmetric PSf/ZIF-8 mixed matrix membrane for CO₂/CH₄ separation," *RSC Advances*, vol. 5, pp. 30206-30215, 2015.
- [39] M. R. Khdayyer, E. Esposito, A. Fuoco, M. Monteleone, L. Giorno, J. C. Jansen, *et al.*, "Mixed matrix membranes based on UiO-66 MOFs in the polymer of

- intrinsic microporosity PIM-1," *Separation and Purification Technology*, vol. 173, pp. 304-313, 2/1/ 2017.
- [40] N. Waheed, A. Mushtaq, S. Tabassum, M. A. Gilani, A. Ilyas, F. Ashraf, *et al.*, "Mixed matrix membranes based on polysulfone and rice husk extracted silica for CO₂ separation," *Separation and Purification Technology*, vol. 170, pp. 122-129, 10/1/ 2016.
- [41] M. U. M. Junaidi, C. P. Leo, S. N. M. Kamal, A. L. Ahmad, and T. L. Chew, "Carbon dioxide removal from methane by using polysulfone/SAPO-44 mixed matrix membranes," *Fuel Processing Technology*, vol. 112, pp. 1-6, 8// 2013.
- [42] S. Rafiq, Z. Man, A. Maulud, N. Muhammad, and S. Maitra, "Separation of CO₂ from CH₄ using polysulfone/polyimide silica nanocomposite membranes," *Separation and Purification Technology*, vol. 90, pp. 162-172, 4/27/ 2012.
- [43] S. M. Sanip, A. F. Ismail, P. S. Goh, T. Soga, M. Tanemura, and H. Yasuhiko, "Gas separation properties of functionalized carbon nanotubes mixed matrix membranes," *Separation and Purification Technology*, vol. 78, pp. 208-213, 4/11/ 2011.
- [44] P. Moradihamedani, N. A. Ibrahim, D. Ramimoghadam, W. M. Z. W. Yunus, and N. A. Yusof, "Polysulfone/zinc oxide nanoparticle mixed matrix membranes for CO₂/CH₄ separation," *Journal of Applied Polymer Science*, vol. 131, 2014.
- [45] S. Kim, T. W. Pechar, and E. Marand, "Poly (imide siloxane) and carbon nanotube mixed matrix membranes for gas separation," *Desalination*, vol. 192, pp. 330-339, 2006.

- [46] X. Guo, H. Huang, Y. Ban, Q. Yang, Y. Xiao, Y. Li, *et al.*, "Mixed matrix membranes incorporated with amine-functionalized titanium-based metal-organic framework for CO₂/CH₄ separation," *Journal of Membrane Science*, vol. 478, pp. 130-139, 2015.
- [47] <http://www.southeastern-automation.com/PDF/Spectra/App%20Notes/Tech%20Note%20-%20Gas%20Phase.pdf>.
- [48] A. Bos, I. G. M. Pünt, M. Wessling, and H. Strathmann, "CO₂-induced plasticization phenomena in glassy polymers," *Journal of Membrane Science*, vol. 155, pp. 67-78, 3/31/ 1999.
- [49] L. Zheng, Y. Wang, X. Wang, X. Wang, H. An, and L. Yi, "The effects of surface modification on the supercapacitive behaviors of carbon derived from calcium carbide," *Journal of Materials Science*, vol. 45, pp. 6030-6037, 2010// 2010.
- [50] Y. Gao, V. Presser, L. Zhang, J. J. Niu, J. K. McDonough, C. R. Pérez, *et al.*, "High power supercapacitor electrodes based on flexible TiC-CDC nano-felts," *Journal of Power Sources*, vol. 201, pp. 368-375, 2012.
- [51] V. Presser, L. Zhang, J. J. Niu, J. McDonough, C. Perez, H. Fong, *et al.*, "Flexible Nano-felts of Carbide-Derived Carbon with Ultra-high Power Handling Capability," *Advanced Energy Materials*, vol. 1, pp. 423-430, 2011.
- [52] J. Xu, Q. Gao, Y. Zhang, Y. Tan, W. Tian, L. Zhu, *et al.*, "Preparing two-dimensional microporous carbon from Pistachio nutshell with high areal capacitance as supercapacitor materials," *Scientific reports*, vol. 4, p. 5545, 2014.

- [53] D. Bhattacharjya and J.-S. Yu, "Activated carbon made from cow dung as electrode material for electrochemical double layer capacitor," *Journal of Power Sources*, vol. 262, pp. 224-231, 2014.
- [54] M. D. Allendorf, "Nanoporous Materials: Chemistry and Applications."
- [55] P. Gupta, *Water vapor adsorption onto nanostructured carbide derived carbon (CDC)*: ProQuest, 2008.
- [56] J. Xu, R. Zhang, P. Chen, and S. Ge, "Effects of adding ethanol to KOH electrolyte on electrochemical performance of titanium carbide-derived carbon," *Journal of Power Sources*, vol. 246, pp. 132-140, 2014.
- [57] S. Urbonaite, *Synthesis and characterisation of carbide derived carbons*: Department of Physical, Inorganic and Structural Chemistry, Stockholm University, 2008.
- [58] S. R. P. Silva, *Properties of amorphous carbon*: Iet, 2003.
- [59] H. Wang, Y. Sun, T. Zhu, W. Wang, and H. Deng, "Adsorption of acetaldehyde onto carbide-derived carbon modified by oxidation," *Chemical Engineering Journal*, vol. 273, pp. 580-587, 8/1/ 2015.
- [60] Y. Otake and R. G. Jenkins, "Characterization of oxygen-containing surface complexes created on a microporous carbon by air and nitric acid treatment," *Carbon*, vol. 31, pp. 109-121, 1993.
- [61] C. Portet, D. Kazachkin, S. Osswald, Y. Gogotsi, and E. Borguet, "Impact of synthesis conditions on surface chemistry and structure of carbide-derived carbons," *Thermochimica Acta*, vol. 497, pp. 137-142, 2010.

- [62] Q. L. Zhuang, T. Kyotani, and A. Tomita, "The change of TPD pattern of O₂-gasified carbon upon air exposure," *Carbon*, vol. 32, pp. 539-540, 1994/01/01 1994.
- [63] Z. R. Yue, W. Jiang, L. Wang, S. D. Gardner, and C. U. Pittman Jr, "Surface characterization of electrochemically oxidized carbon fibers," *Carbon*, vol. 37, pp. 1785-1796, // 1999.
- [64] U. Zielke, K. J. Hüttinger, and W. P. Hoffman, "Surface-oxidized carbon fibers: I. Surface structure and chemistry," *Carbon*, vol. 34, pp. 983-998, 1996.
- [65] A. Derylo-Marczewska, B. Buczek, and A. Swiatkowski, "Effect of oxygen surface groups on adsorption of benzene derivatives from aqueous solutions onto active carbon samples," *Applied Surface Science*, vol. 257, pp. 9466-9472, 9/1/ 2011.
- [66] B. Suart, "Infrared Spectroscopy: Fundamental and Applications," ed: John Wiley & Sons, Ltd, 2004.
- [67] M. Sevilla and R. Mokaya, "Activation of carbide-derived carbons: a route to materials with enhanced gas and energy storage properties," *Journal of Materials Chemistry*, vol. 21, pp. 4727-4732, 2011.
- [68] P. Moradihamedani, N. A. Ibrahim, W. M. Z. W. Yunus, and N. A. Yusof, "Study of morphology and gas separation properties of polysulfone/titanium dioxide mixed matrix membranes," *Polymer Engineering & Science*, vol. 55, pp. 367-374, 2015.
- [69] O. Kazak, A. Tor, I. Akin, and G. Arslan, "Preparation of new polysulfone capsules containing Cyanex 272 and their properties for Co (II) removal from

- aqueous solution," *Journal of Environmental Chemical Engineering*, vol. 3, pp. 1654-1661, 2015.
- [70] M. I. Baig, P. G. Ingole, W. K. Choi, S. R. Park, E. C. Kang, and H. K. Lee, "Water vapor permeation behavior of interfacially polymerized polyamide thin film on hollow fiber membrane substrate," *Journal of the Taiwan Institute of Chemical Engineers*, vol. 60, pp. 623-635, 2016.
- [71] P. Lu, S. Liang, T. Zhou, X. Mei, Y. Zhang, C. Zhang, *et al.*, "Layered double hydroxide/graphene oxide hybrid incorporated polysulfone substrate for thin-film nanocomposite forward osmosis membranes," *RSC Advances*, vol. 6, pp. 56599-56609, 2016.
- [72] A. D. Kiadehi, M. Jahanshahi, A. Rahimpour, and S. A. A. Ghoreyshi, "The effect of functionalized carbon nano-fiber (CNF) on gas separation performance of polysulfone (PSf) membranes," *Chemical Engineering and Processing: Process Intensification*, vol. 90, pp. 41-48, 4// 2015.
- [73] N. N. Rupiasih, H. Suyanto, M. Sumadiyasa, and N. Wendri, "Study of effects of low doses UV radiation on microporous polysulfone membranes in sterilization process," 2013.
- [74] M. A. Aroon, A. F. Ismail, M. M. Montazer-Rahmati, and T. Matsuura, "Morphology and permeation properties of polysulfone membranes for gas separation: Effects of non-solvent additives and co-solvent," *Separation and Purification Technology*, vol. 72, pp. 194-202, 2010.

- [75] B. Zornoza, C. Téllez, and J. Coronas, "Mixed matrix membranes comprising glassy polymers and dispersed mesoporous silica spheres for gas separation," *Journal of Membrane Science*, vol. 368, pp. 100-109, 2/15/ 2011.
- [76] N. Jusoh, Y. F. Yeong, W. L. Cheong, K. K. Lau, and A. M. Shariff, "Facile fabrication of mixed matrix membranes containing 6FDA-durene polyimide and ZIF-8 nanofillers for CO₂ capture," *Journal of Industrial and Engineering Chemistry*, vol. 44, pp. 164-173, 2016.
- [77] H. Sun, T. Wang, Y. Xu, W. Gao, P. Li, and Q. J. Niu, "Fabrication of polyimide and functionalized multi-walled carbon nanotubes mixed matrix membranes by in-situ polymerization for CO₂ separation," *Separation and Purification Technology*, vol. 177, pp. 327-336, 4/28/ 2017.
- [78] Q. Xin, H. Wu, Z. Jiang, Y. Li, S. Wang, Q. Li, *et al.*, "SPEEK/amine-functionalized TiO₂ submicrospheres mixed matrix membranes for CO₂ separation," *Journal of Membrane Science*, vol. 467, pp. 23-35, 2014.
- [79] J. C. Poshusta, R. D. Noble, and J. L. Falconer, "Temperature and pressure effects on CO₂ and CH₄ permeation through MFI zeolite membranes," *Journal of Membrane Science*, vol. 160, pp. 115-125, 7/15/ 1999.
- [80] W.-H. Lin and T.-S. Chung, "Gas permeability, diffusivity, solubility, and aging characteristics of 6FDA-durene polyimide membranes," *Journal of Membrane Science*, vol. 186, pp. 183-193, 5/30/ 2001.

]

Vitae

Name :Musa Olajide Najimu |

Nationality :Nigerian |

Date of Birth :7/18/1988|

Email :musanajimu@gmail.com|

Address :Ile-Ife, Osun state, Nigeria|

Academic Background :B.S.c Chemical Engineering (2008 – 2013),
|Obafemi Awolowo University, Ile-Ife, Nigeria|